CHAPTER 4

Coordination polymeric fluorescent gel: effect of removal of branch substituents of the central core over properties and effect of spacer length variation over metallogel behavior

4.1 Introduction

Synthesis of a chain length selective metallogelation of bis-acylhydrazone included Schiff base ligands obtained from a series of homologous dicarboxylate derivative in the presence of LiOH and Zn^{2+} and Cd^{2+}. The results presented are quite significant and different from other reported coordination polymer gels in a number of ways.

(a) A number of reports selective to functional groups, stereochemistry, the relative position of donor/acceptor, and active metal center with bisacylhydrazones with their d^{10} complexes are available. However, a metallogel involving a change in core with a strategy towards tuning of morphological behavior has not been reported. It has been categorically observed that change in flexibility of core could alter the mode of complexation followed by gelation.

(b) Till to date, the effect of chain length is only explored in organic gels and none of the research has been carried over in the field of metallogel. Reckoning this observation, strategically, we framed the effect of variation in flexible spacer length over structural and optical properties of metallogel.

(c) A non-emissive solution of the gelator became emissive upon deprotonation, followed by metal addition due to CHEF along with the AIE-ACQ effect.

(d) Fluorescence emission and UV-vis studies indicate the presence of aggregation.

(e) Rheological studies indicated that sharp phase transition via gel-semi sol-solid at T_{gel} while gel-sol phase transition at yield stress. Variable temperature fluorescence studies also support the rheological data analysis.

Supramolecular gels are the unique class of smart materials attained immense interest in recent years, mainly due to responsiveness to external perturbations, nanostructure, optical, and Physico-chemical behavior [Quan *et al*. (2011), Segarra-Maset *et al*. (2013)]. Among them, 'metallogel' with the metal centre through coordinate or covalent bonds as well as weak interactions between molecules construct functionalities beyond the constituent molecules and craft extended network with voluminous entrapment of solvent [Tam *et al*. (2013), Dastidar *et al.* (2016), Diring *et al.* (2009)]. Metallogel comprises a large array of applications in catalysis, drug-delivery system, sensing devices, bio-imaging and photo-physical behaviour [Lin *et al.* (2014), Yang *et al.* (2010), Xing *et al.* (2002)]. The gelation behaviour of a metallogel depends upon the diversity among the molecular structure with respect to sequence, stereochemistry of organic linker and choice of metal centres as well as the polarity of solvents. On the other hand, the metallogel properties can be tuned with small modifications at the molecular level [Dawn *et al.* (2012), Pandey *et al.* (2019), Chow & Zhang (2005), Makarević *et al.* (2003)]. A number of reports selective to functional groups, stereochemistry, the relative position of donor/acceptor and active metal centre with bisacylhydrazones with their d^{10} complexes are available. However, a metallogel involving a change in core with a strategy towards tuning of morphological behaviour has not been reported. It has been categorically observed that change in flexibility of core could alter the mode of complexation [Lu *et al.* (2016), Chen *et al.* (2015)]. Effect of variation of chain/spacer/core length over aggregation and/or gelation is quite an attractive topic to scientists [Ogi *et al.* (2016), Dai *et al.* (2000), Heinz *et al.* (2007), Miao *et al.* (2015), Peng *et al.* (2008), Clark *et al.* (1989), Zhu & Dordick (2006), Nagasawa *et al.* (2015)]. A number of reports are available explaining the effect of spacer length over aggregation as well as

gelation. In conclusion, spacer length has a quite clear effect over gelation. Further, in gel chemistry, all the reports available to date are only explored in organic gels and none of the research has been carried over in the field of metallogel. Reckoning this observation, strategically, we framed the effect of variation in flexible spacer length over structural and optical properties of metallogel.

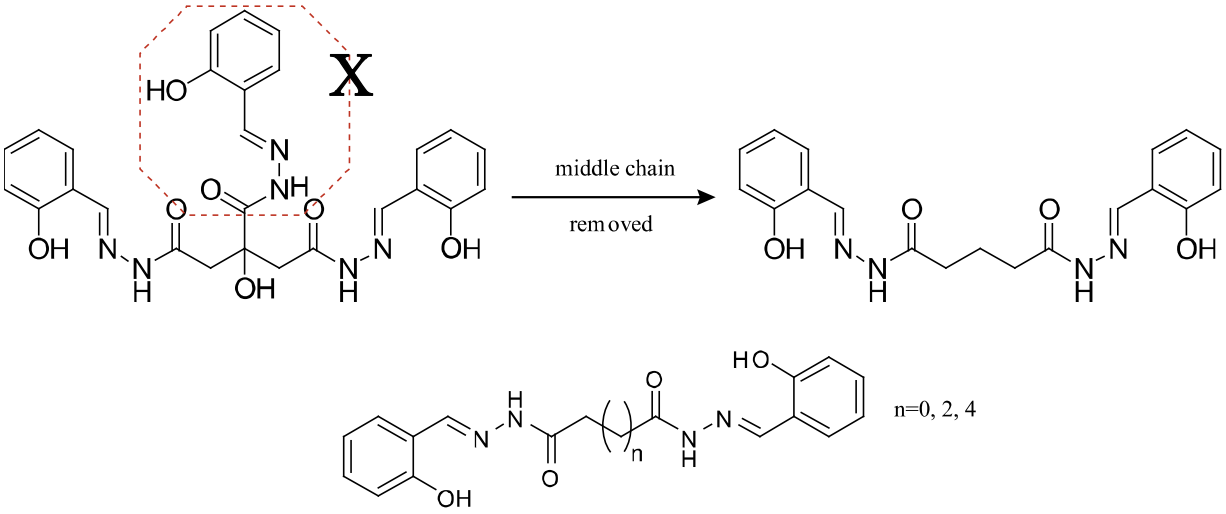

Figure 4.1 Origin of the idea behind the synthesis of gelator formed by adipic acid

4.2 Synthesis

4.2.1 Synthesis of Bis(acylhydrazones) (BHN; n=4)

To a methanolic solution of Adipic acid (1.00 g, 6.60 mmol), a few drops of conc. Sulphuric acid was added as a catalyst, and the reaction mixture was refluxed overnight. In vacuo reduction in volume with mild heating was done to afford dimethyl adipate as a clear oil. Dimethyl adipate (1.0g, 6.8 mmol), reacted with hydrazine hydrate (0.68 g, 13.6 mmol) in methanol and refluxed for 6 hours. White crystals were obtained on cooling down to room

temperature that was secluded by filtration, washed with diethyl ether and dried in a desiccator. In a similar way, Oxaloyl dihydrazone BHN (n=0); Succinoyl dihydrazone BHN (n=2) and suberoyl dihydrazone BHN (n=6) were also prepared using oxalic, succinic and suberic acid respectively.

4.2.2 Synthesis of AL

To a methanolic suspension of BHN (n=4) (1.00g, 6.8 mmol), 2 mL water is added to obtain a clear solution. 2-hydroxybenzaldehyde (1.67g, 13.6 mmol) was added to this solution and refluxed for 1 hour. The precipitate obtained after cooling to room temperature was filtered, thoroughly washed with Chloroform, methanol, and Hexane to afford a white solid (AL), Yield 1.74g (81%). Due to deprived solubility of the neutral form, UV-vis measurements were performed by dissolving the solid in DMF in the presence of 1 Equivalent of LiOH [Golla *et al.* (2016)].

All supporting ligand was synthesized by following a similar procedure to AL, only by using their respective hydrazones.

4.2.3 Synthesis of OL

To a methanolic suspension of BHN (n=0) (1.00g, 6.8 mmol), 2 mL water is added to obtain a clear solution. 2-hydroxybenzaldehyde (1.67g, 13.6 mmol) was added to this solution and refluxed for 1 hour. The precipitate obtained after cooling to room temperature was filtered, thoroughly washed with Chloroform, methanol, and Hexane to afford a white solid (AL), Yield 1.74g (81%). Due to deprived solubility of the neutral form, UV-vis

measurements were performed by dissolving the solid in DMF in the presence of 1 Equivalent of LiOH.Yield 2.1g (76.1%).

4.2.4 Synthesis of ML

To a methanolic suspension of BHN (n=1) (1.00g, 6.8 mmol), 2 mL water is added to obtain a clear solution. 2-hydroxybenzaldehyde (1.67g, 13.6 mmol) was added to this solution and refluxed for 1 hour. The precipitate obtained after cooling to room temperature was filtered, thoroughly washed with Chloroform, methanol, and Hexane to afford a white solid (AL), Yield 1.74g (81%). Due to deprived solubility of the neutral form, UV-vis measurements were performed by dissolving the solid in DMF in the presence of 1 Equivalent of LiOH.Yield 1.91g (74.1%).

4.2.5 Synthesis of SL

To a methanolic suspension of BHN (n=2) (1.00g, 6.8 mmol), 2 mL water is added to obtain a clear solution. 2-hydroxybenzaldehyde (1.67g, 13.6 mmol) was added to this solution and refluxed for 1 hour. The precipitate obtained after cooling to room temperature was filtered, thoroughly washed with Chloroform, methanol, and Hexane to afford a white solid (AL), Yield 1.74g (81%). Due to deprived solubility of the neutral form, UV-vis measurements were performed by dissolving the solid in DMF in the presence of 1 Equivalent of LiOH. Yield 1.98g (81.6%).

4.2.6 Synthesis of GL

To a methanolic suspension of BHN (n=3) (1.00g, 6.8 mmol), 2 mL water is added to obtain a clear solution. 2-hydroxybenzaldehyde (1.67g, 13.6 mmol) was added to this

solution and refluxed for 1 hour. The precipitate obtained after cooling to room temperature was filtered, thoroughly washed with Chloroform, methanol, and Hexane to afford a white solid (AL), Yield 1.74g (81%). Due to deprived solubility of the neutral form, UV-vis measurements were performed by dissolving the solid in DMF in the presence of 1 Equivalent of LiOH. Yield 1.77g (76.9%).

4.2.7 Synthesis of PL

To a methanolic suspension of BHN (n=5) (1.00g, 6.8 mmol), 2 mL water is added to obtain a clear solution. 2-hydroxybenzaldehyde (1.67g, 13.6 mmol) was added to this solution and refluxed for 1 hour. The precipitate obtained after cooling to room temperature was filtered, thoroughly washed with Chloroform, methanol, and Hexane to afford a white solid (AL), Yield 1.74g (81%). Due to deprived solubility of the neutral form, UV-vis measurements were performed by dissolving the solid in DMF in the presence of 1 Equivalent of LiOH. Yield 1.65g (78.3%).

4.2.8 Synthesis of SUL

To a methanolic suspension of BHN (n=6) (1.00g, 6.8 mmol), 2 mL water is added to obtain a clear solution. 2-hydroxybenzaldehyde (1.67g, 13.6 mmol) was added to this solution and refluxed for 1 hour. The precipitate obtained after cooling to room temperature was filtered, thoroughly washed with Chloroform, methanol, and Hexane to afford a white solid (AL), Yield 1.74g (81%). Due to deprived solubility of the neutral form, UV-vis measurements were performed by dissolving the solid in DMF in the presence of 1 Equivalent of LiOH. Yield 1.59g (78.7%).

4.2.9 Synthesis and Characterization of APL

It was synthesized following the similar procedure described for AL, using 4-hydroxybenzaldehyde (1.67g, 13.6 mmol) instead of 2-hydroxybenzaldehyde. Yield 1.70g (79.4%).

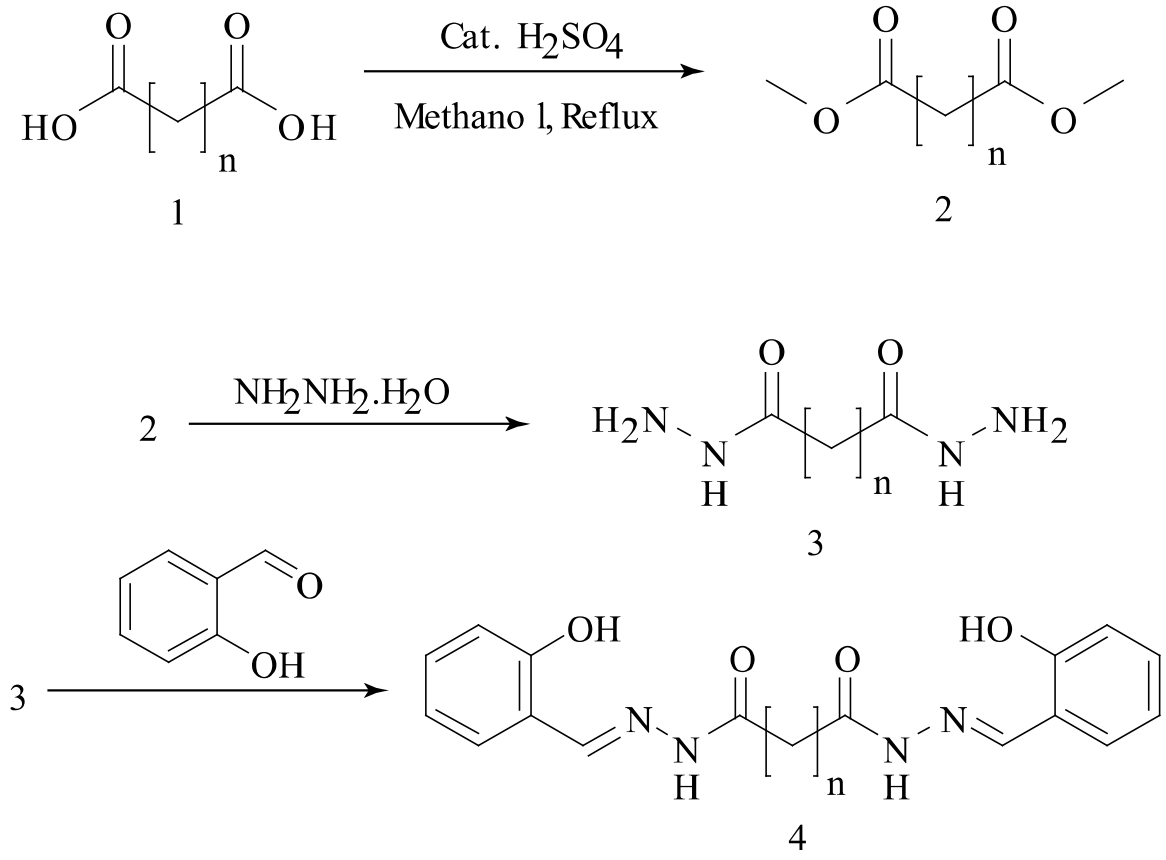

Scheme 4.1 Synthetic scheme for the formation of Adipic acid homologue derivative ligands

Various Homologous Isomers

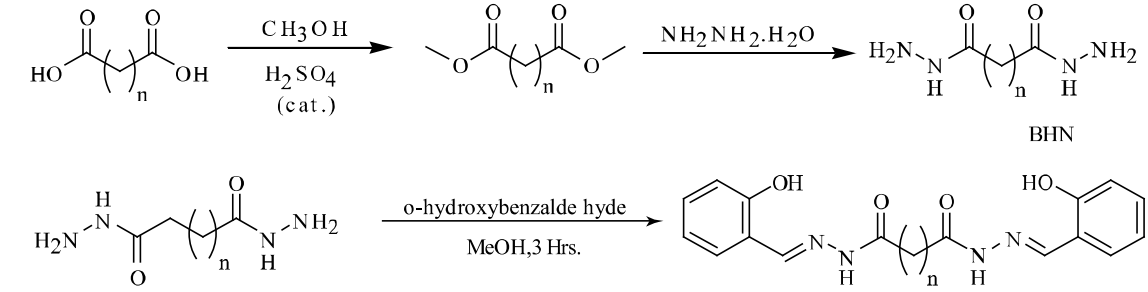

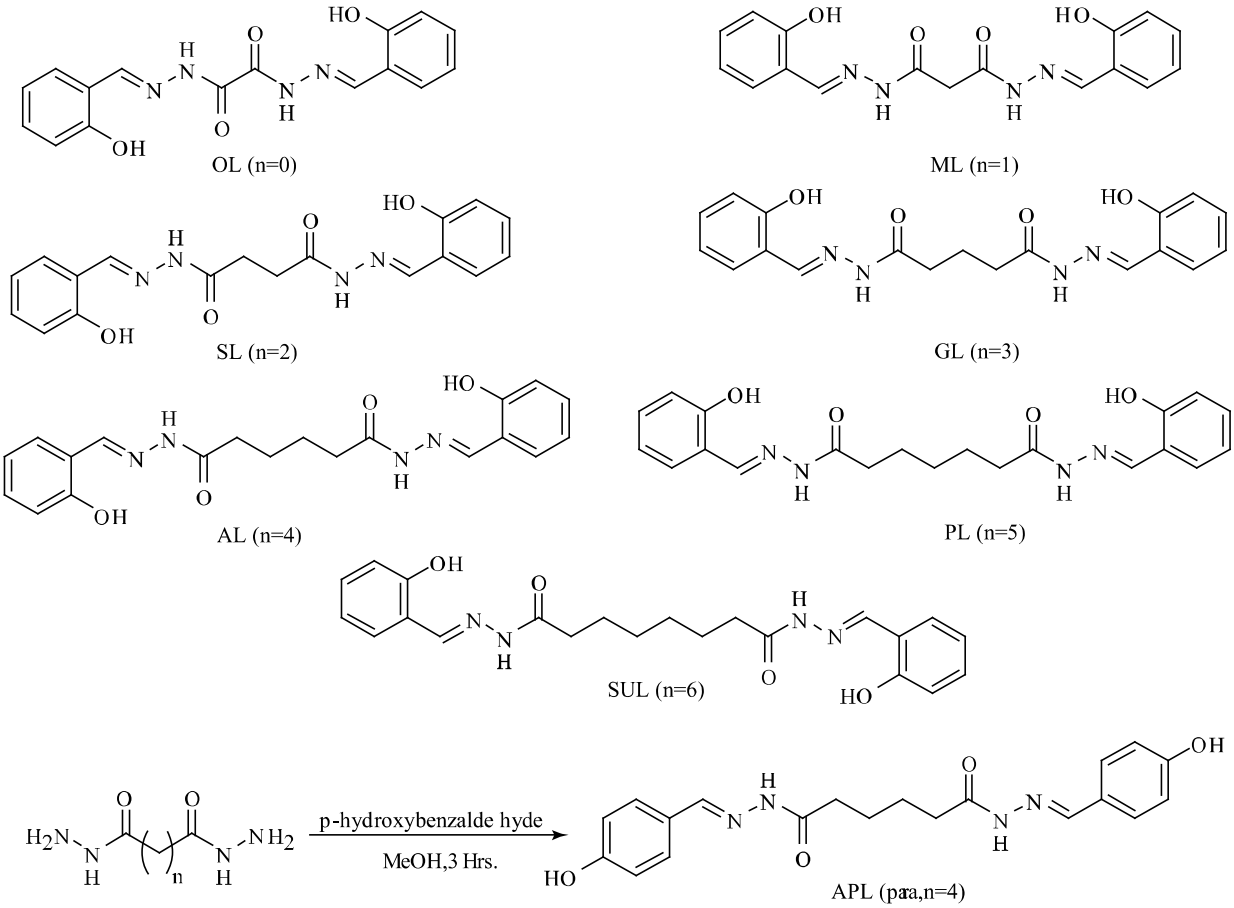

Scheme 4.2 all homologous ligands derived from dicarboxylate derivatives

To explore the effect of spacer over metallogel synthesis, we have engineered bis-acyl-hydrazone containing ligands based upon homologous series of a saturated dicarboxylic acid, consisting variable methyl spacers (from n=0 to n=6) between two salicylaldimine ends. Thus, these ligand exhibit flexibility created by spacers and two important sets of N,N,O coordination sites having pseudo amide functionalities, providing an excellent platform to achieve specific gelation and fluorescence behavior.

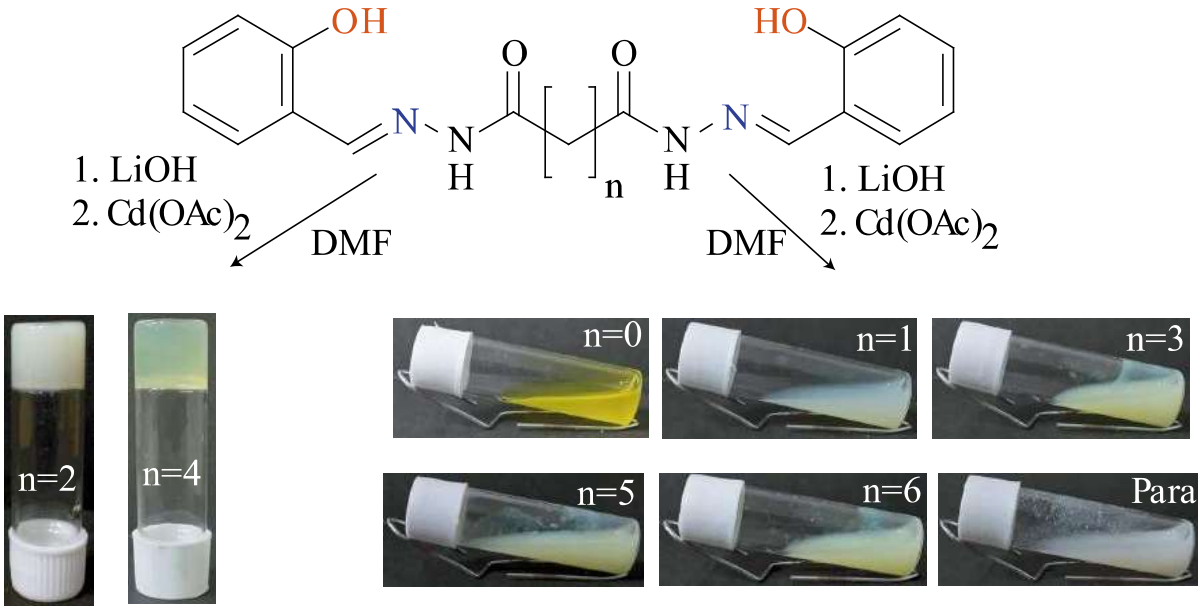

Figure 4.2 Chain length specific gelation behavior of saturated dicarboxylic acid analogues (n=0 to 6 and para isomer) where gelation observed only for n=2 and n=4

4.3 Instrumentation

Sonicator used was Selec 1.5 L 50Hz/DTC (0.45 W/cm^2, 50 kHz) sonicator. Elemental analyses for carbon, hydrogen and nitrogen were acquired on an Exeter CHN Analyzer CE-440. FT-IR and electronic absorption spectra were obtained on a PerkinElmer Spectrum 100 and Thermo scientific EVOLUTION 201 spectrophotometers, respectively. Photoluminescence spectra were acquired on a Perkin Elmer LS 55 spectrophotometer. The lifetime measurements were made using a TCSPC system from Horiba Yovin (Model: Fluorocube-01-NL). The samples were excited at 378 nm using a picosecond diode laser (Model: Pico Brite-375L) and data analysis was performed using IBH DAS (version 6, HORIBA Scientific, Edison, NJ) decay analysis software. ^{1}H NMR spectra were obtained on a Bruker AVANCE III HD 500 spectrometer. Electrospray ionization mass (ESI-MS) spectra were recorded on a Waters (Micromass MS Technologies) QTof Premier. Thermal Gravimetric analysis data was acquired on a NETZSCH STA 449 F3 at a heating rate of 5 °C min^{-1} under a nitrogen atmosphere. TEM images and AFM were captured using a JEOL JEM 2100 and NT-MDT NTEGRA PRIMA, respectively. Powder XRD data were collected on Rigaku MiniFlex 600 Detector D-tex ultra between angle 2θ = 5-80°. Solution electrical conductivity was measured on a Eutech Instruments CON 5/TDS 5 Conductivity Meter. The instrument was calibrated with the standard solution. Rheology of sonometallogel was performed on Anton Paar MCR 702 Twin Drive Rheometer.

The ligand (AL) needed for the synthesis of Coordination polymer Gel (CPG) was synthesized and characterized following our earlier method. The characterization details of OL, ML, SL, GL, AL, PL, SUL and APL along with coordination polymer gel, are described

below. Elemental analyses for C, H and N, were obtained on a Thermo Finnigan FLASH EA 1112 series analyzer. Infrared and UV-visible absorption spectra were acquired on a Perkin Elmer-Spectrum 100 FT-IR and Thermo scientific Evolution 200 spectrophotometers, respectively.

4.3.1 UV-vis Study

A stock solution of AL with LiOH (50 μM) for an electronic absorption study was prepared in DMF. Solutions of Zinc Acetate $Zn(OAc)_2 \cdot 2H_2O$, Cadmium Acetate $Cd(OAc)_2 \cdot 2H_2O$, Cadmium Nitrate $Cd(NO_3)_2.4H_2O$ and Cadmium perchlorate $Cd(ClO_4)_2.XH_2O$ (1M) were also prepared in DMF. In a typical titration, the solution of AL deprotonated with LiOH was taken in a quartz cuvette (3.0 mL; path length, 1 cm), and the metal solution was added gradually with the help of a micropipette. After every addition, proper mixing was performed and spectra were taken. Similar titration experiments at gelation conditions were done for supporting ligand too.

4.3.2 Fluorescence Study

Photoluminescence spectra were acquired on a Perkin Elmer LS 55 spectrophotometer. The lifetime measurements were made using a TCSPC system from Horiba Yovin (Model: Fluorocube-01-NL). The samples were excited at 378 nm using a picoseconds diode laser (Model: Pico Brite-375L), and data analysis were performed using IBH DAS (version 6, HORIBA Scientific, Edison, NJ) decay analysis software.

4.3.3 Rheological Study

Measurements were performed on a stress-controlled Rheometer (Anton Paar TWINE Rheometer MCR 702) equipped with parallel stainless steel plates (20 mm diameter, 1.0 mm gap). All experiments were carried out on 1% w/v freshly prepared metallogel. Linear viscoelastic region of samples was determined by computing storage modulus, G' (a measure of elasticity and ability of energy storage) and loss modulus, G'' (the ability of a material to dissipate energy) as a function of stress amplitude (Dynamic oscillatory frequency of 1 rad s^{-1}). Following experiments were conducted: increasing amplitude of oscillation up to 100% apparent strain on shear, time and frequency sweep at 25°C (20 min and from 0.1 to 100 rad s^{-1}, respectively) and heating run to 160° C at a scan rate of 5° C/min. All experiments were conducted twice.

4.3.4 NMR study

Three different conformational isomers have existed in ^{1}H NMR analysis but those were immaculated upon addition of alkali base [Levrand *et al*. (2007)].

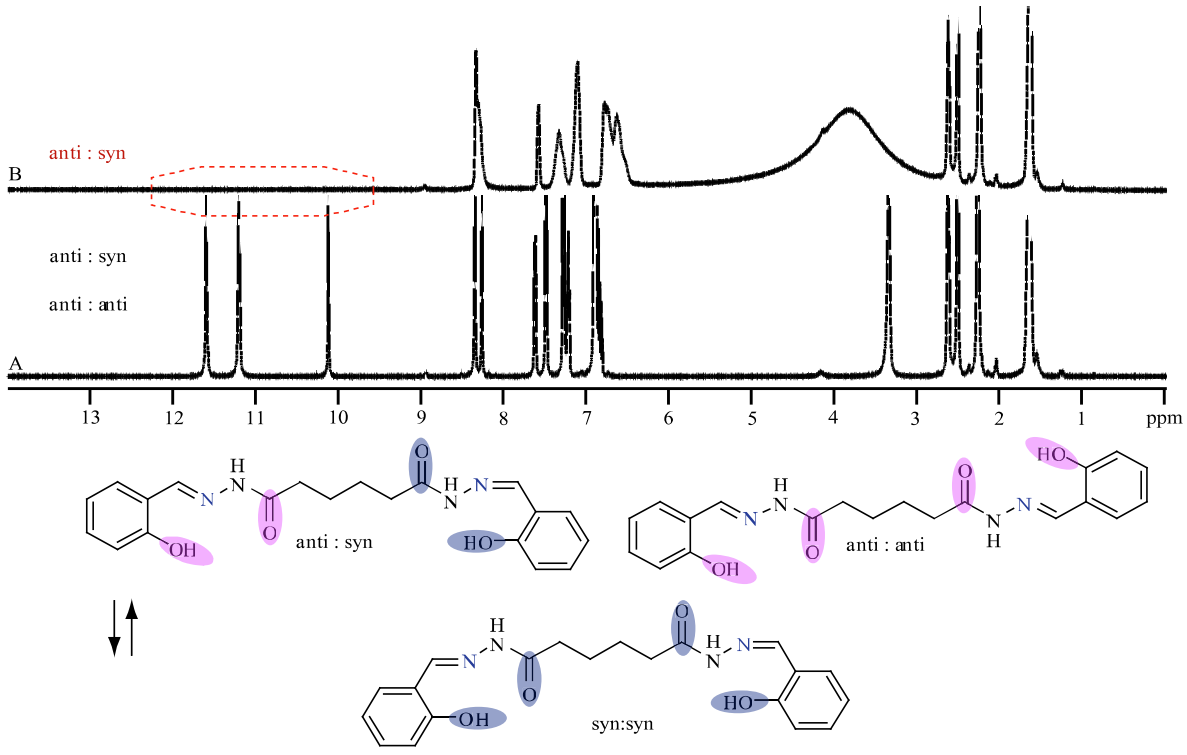

Figure 4.3 ^{1}H NMR spectra (500 MHz, DMSO-d6, 298 K) for (A) isomer ADL, where sketch diagram of three plausible conformers anti-anti, syn-anti and syn-syn are shown (B) three plausible conformers of isomer AL converted into single conformer anti-syn upon treatment with LiOH. The labile protons regions –NH and –OH were deprotonated after treatment with LiOH (deprotonated region shown by the red dotted circle)

In addition to selectivity towards specific spacer length and metal center, counter ion specificity was also monitored. Upon addition of one equivalent of various Cadmium and Zinc salt (CH_3COO^-, NO_3^-, ClO_4^- and SO_4^{2-}) H_4AL and H_4SL could gel DMF only in the presence of acetate salt indicating the anion selectivity towards gelation [Wu *et al.* (2015)].

Table 4.1 The solubility and gelation ability of Supporting ligands in DMF and Alkali metals with $Zn(OAc)_2.2H_2O$ and $Cd(OAc)_2$

Ligand	LiOH	NaOH	KOH	CsOH	$Zn(OAc)_2.2H_2O$	$Cd(OAc)_2.2H_2O$
OL (n=0)	S	S	S	S	S	S
ML (n=1)	S	S	S	S	SP	SP
SL (n=2)	S	S	S	S	G	G
GL (n=3)	S	S	S	S	GP	GP
PL (n=5)	S	S	S	S	SP	SP
SUL (n=6)	S	S	S	S	SP	SP
APL (para)	S	S	S	S	SP	SP

S = Soluble, G = Gel, SP = Suspension, GP = Gelatinous ppt.

Table 4.2 Gelation ability of AL with all alkali metals in DMF (in the presence of Cd(II)/Zn(II) acetate)

Solvent	LiOH	NaOH	KOH	CsOH
Water	SP	SP	SP	SP
Methanol	S	S	S	S
Ethanol	S	S	S	S
DMSO	S	S	S	S
DMF	G	G	G	G
Acetone	I	I	I	I
Ethyl Acetate	I	I	I	I
THF	I	I	I	I
DCM	I	I	I	I
Chloroform	I	I	I	I
1,4-dioxane	I	I	I	I
Hexane	I	I	I	I

I = Insoluble, S = Soluble, G = Gel, SP= Suspension

4.3.5 Mechanical Properties of gel

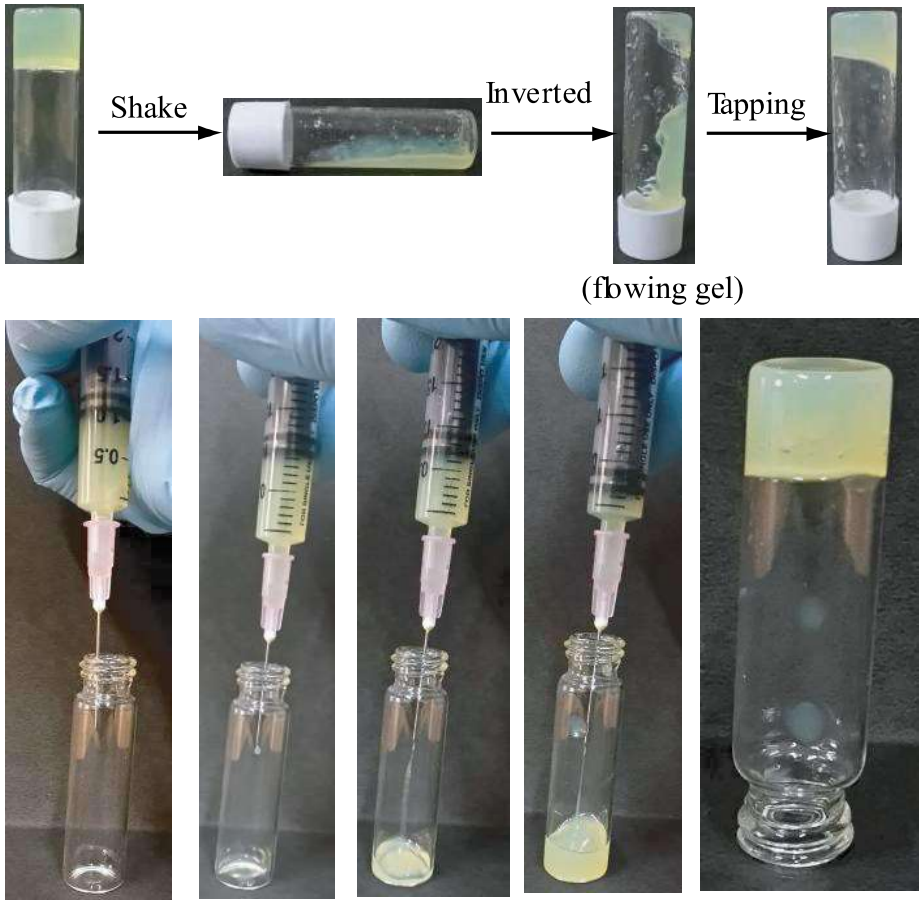

Figure 4.4 Gel shows mechanical stimuli-responsive behavior and also injectibility towards the desired location to check ease of transportation

4.3.6 Degree of Freedom

Stoichiometric ratios of other homologues were found to be nearly the same but gelation observed only in even spacers (other than n=0) where both tridentate domains of the ligand are anti to each other is again an indication of the role of odd/even spacers towards gelation behaviour.

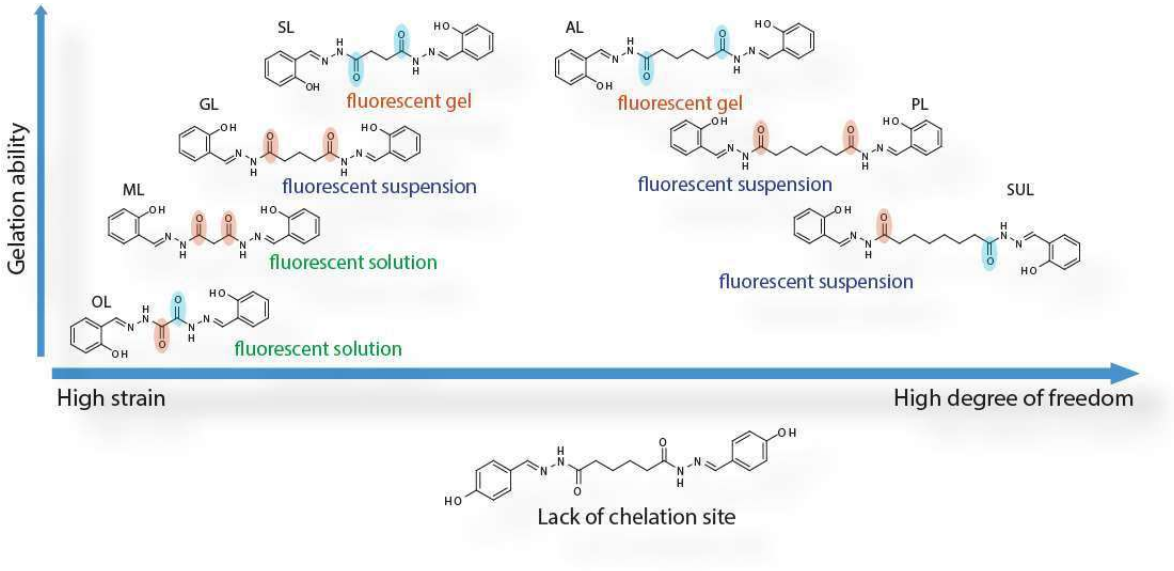

Figure 4.5 Schematic representation of gelation ability of various homologues with $Cd(OAc)_2.2H_2O$ and $Zn(OAc)_2.2H_2O$; high strain and a higher degree of freedom with variable chain length cease the gelation ability

4.3.7 Gelation behavior and visible optical properties

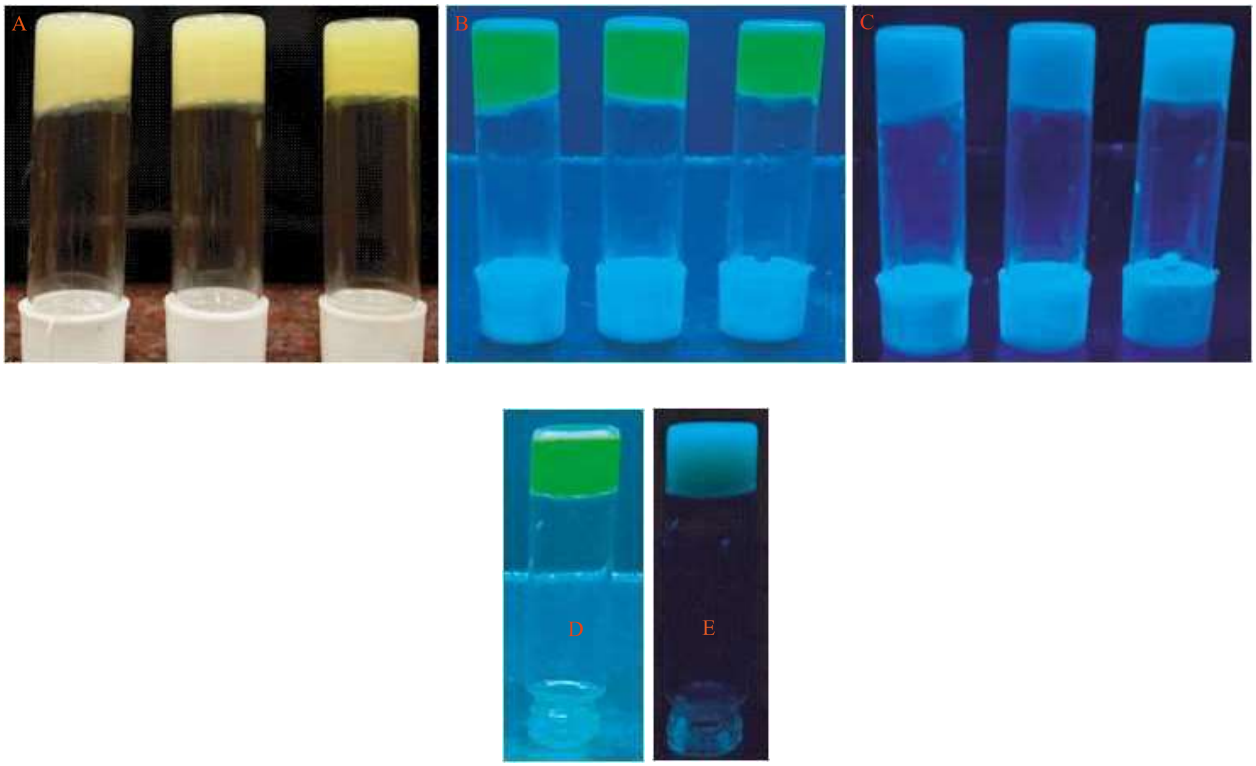

Figure 4.6 Photographs of CPG: From left to right- In inverted vial (a) Lithium, (b) Sodium and (c) Potassium gel with $Cd(OAc)_2 \cdot 2H_2O$, in inverted vial under (A: Under naked eye), (B: In short UV), (C: UV light, λ= 365 nm)

4.3.8 Solid State Fluorescence

The effect of spacer moiety over fluorescence and complexation behaviour was also evidenced by solid-state reaction of H_4OL, H_4SL and H_4AL with LiOH and $Cd(OAc)_2$. Upon grinding H_4OL with LiOH it emits weak yellow fluorescence which enhances significantly upon grinding with a metal salt. H_4SL under similar condition exhibits mild blue fluorescence while H_4AL exhibit strong blue fluorescence in solid-state.

Figure 4.7 Photographs of solid-state reaction product : From top to bottom on glass slide left Ligand + Lithium + $Cd(OAc)_2 \cdot 2H_2O$ (A : Under naked eye), (B : In short UV), (C : UV light , λ= 365 nm); right Ligand + Lithium + $Zn(OAc)_2 \cdot 2H_2O$ (A : Under naked eye), (B : In short UV), (C : UV light , λ= 365 nm)

4.3.9 Morphology

Morphology revealed by H_4AL derived gel was also inline to the above statement where SEM revealed a bunch of extended and interconnected fibres with close-knitted appearance. TEM study on diluted metallogel revealed the three-dimensional (3-D) network of nano-fibres of about ~30 nm in average diameter with intermingled appearance [Yan *et al.* (2014), Yu *et al*. (2015)].

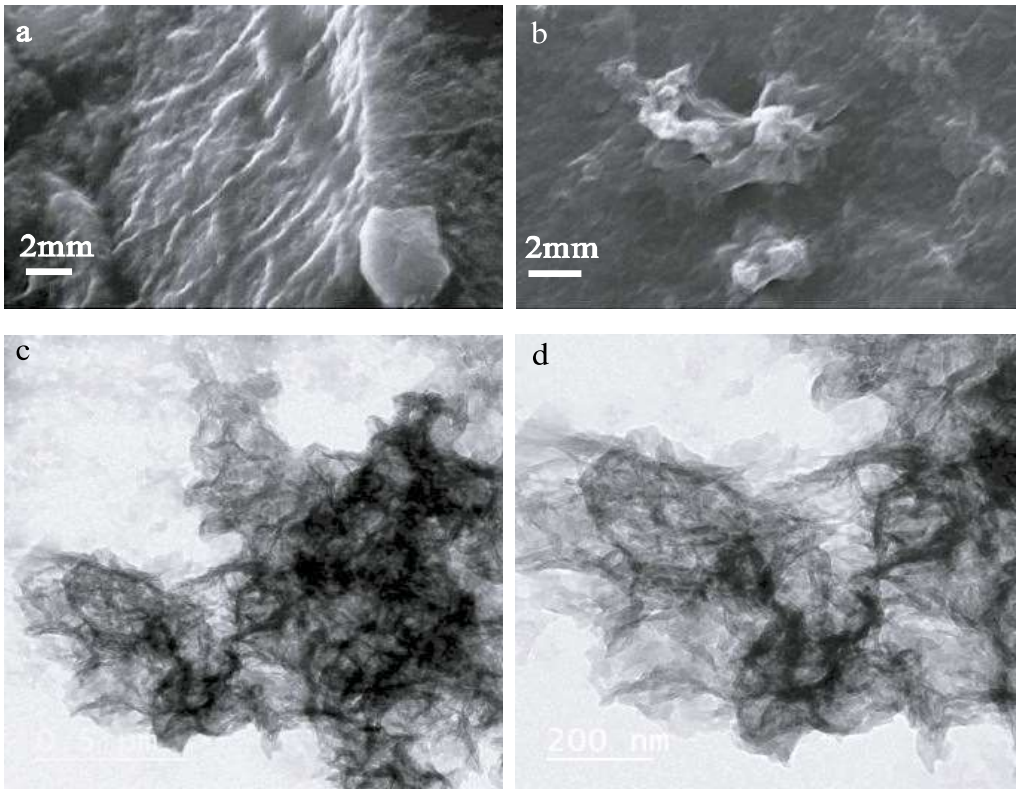

Figure 4.8 TEM images of diluted samples (A, B) reveals long-range nano-fibers with an average diameter of ~30 nm

4.3.10 PXRD

During the synthesis of coordination polymer, metal center with an obligatory geometry mostly binds to organic anions, flexible ligand when linked to the metal centers lacking tendency to form periodic networks. PXRD patterns for H_4AL in 2θ range 5-35° showed the crystalline nature of ligand while the amorphous nature of xerogel. However, the simultaneous crystallization of Li^+/K^+ and Cd^{2+}/Zn^{2+} as Li_2CO_3/K_2CO_3 (23.2°/24.5°) and CdO/ZnO (11.7°/12.22°) respectively, cannot be ruled out.

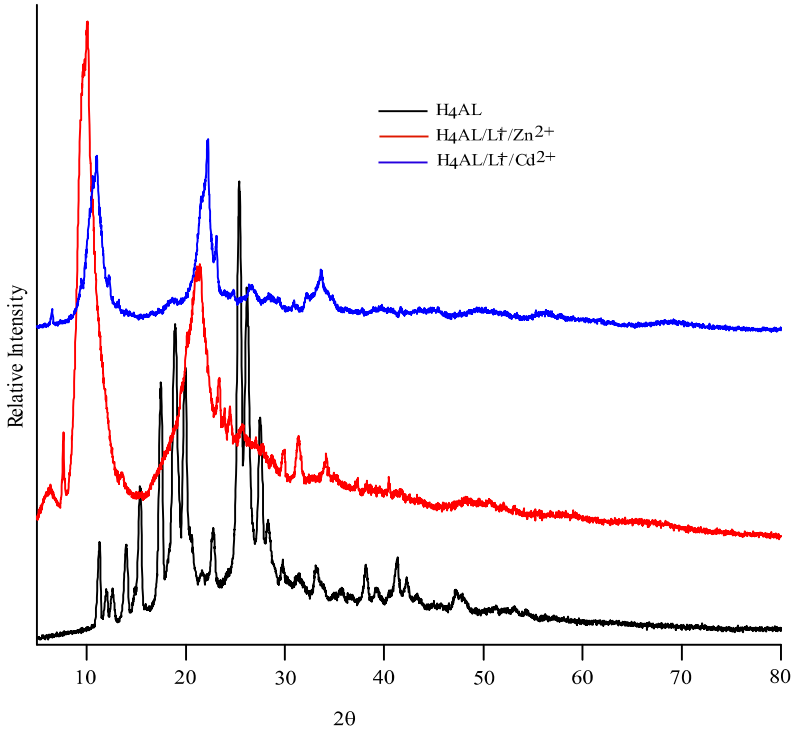

Figure 4.9 Powder X-ray diffraction pattern of isomer AL (black line), AL/LiOH/Zn(II) (red line), AL/LiOH/Cd(II) (blue line), AL/KOH/Zn(II) (green line), AL/KOH/Cd(II) (pink line) indicating the loss of crystalline behavior towards amorphous nature upon complexation and gelation (xerogel)

4.3.11 UV-vis Spectroscopy

To prove the complexation between H_4AL and Zn^{2+}/Cd^{2+} as well as gelation behavior, we executed detailed electronic absorption studies. Exposition of two vividly coupled bands by H_4AL ($1x10^{-5}$ M, DMF, 298 K) at λ_{max}=280 nm and 291 nm are accredited to intra ligand π-π* transition while a less intense band at 320 nm endorsed n-π* transition. Alternatively, splitting of the peak at 280 and 291 nm elucidate dissimilar planarity of both hydrazones i.e., both free hydrazones exist in anti-cis configuration. Insignificant change in spectra was observed upon deprotonation of H_4AL ($1x10^{-5}$ M, DMF) with 4 eq. LiOH, while upon aliquot addition of either $Cd(OAc)_2$ or $Zn(OAc)_2$ ($1x10^{-3}$ M, DMF) to this solution, disappearance of band at 320 nm was observed with ratiometric emergence of a new peak at 382 nm ($\Delta\lambda$ = 62 nm) (Figure 4.10). Two nice isosbestic points at 305 and 344 nm indicate the presence of equilibrium between two species during their transformation to the coordination complex. The endpoint of UV titrations was found to be 1.0-1.2 equivalent indicated the formation of coordination complex between Cd(II)/Zn(II) with H_4AL at 1:1 ratio. Stoichiometry model for Cd^{2+} complexation in both gelators H_4AL and H_4SL demonstrated through Job's plot was found in good agreement to above spectroscopic result where both gelling combinations were found close to 1:1 metal to ligand ratio which is bit different from rest of the non-gelling combinations [Hosseini-Monfared *et al.* (2014), Basumatary *et al.* (2015)].

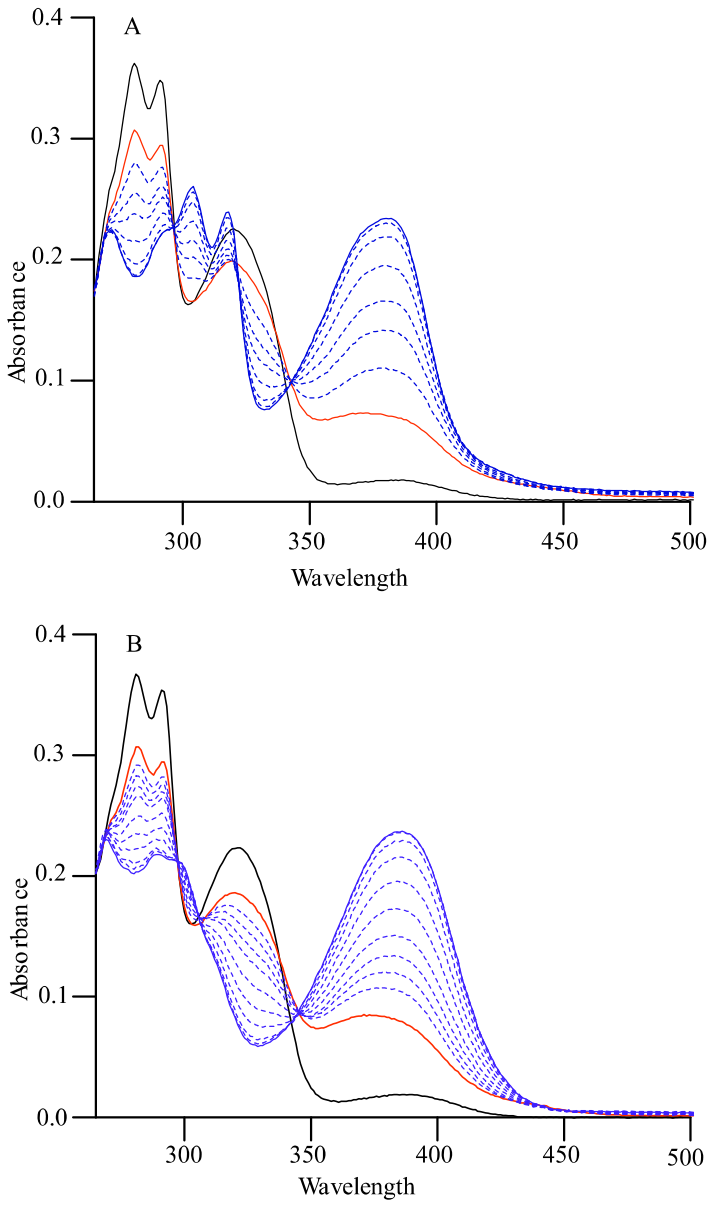

Figure 4.10 UV-vis titrations in DMF (A) ligand AL (black line; λmax 322 nm; $1x10^{-5}$ M), deprotonation with LiOH (2 equiv., red line) and upon aliquot addition of $Cd(OAc)_2$ (blue line) band corresponding to ligand diminishes with appearance of new band at 378 nm, coincidently with an isosbestic point; similar titration experiments performed with (B) $Zn(OAc)_2$

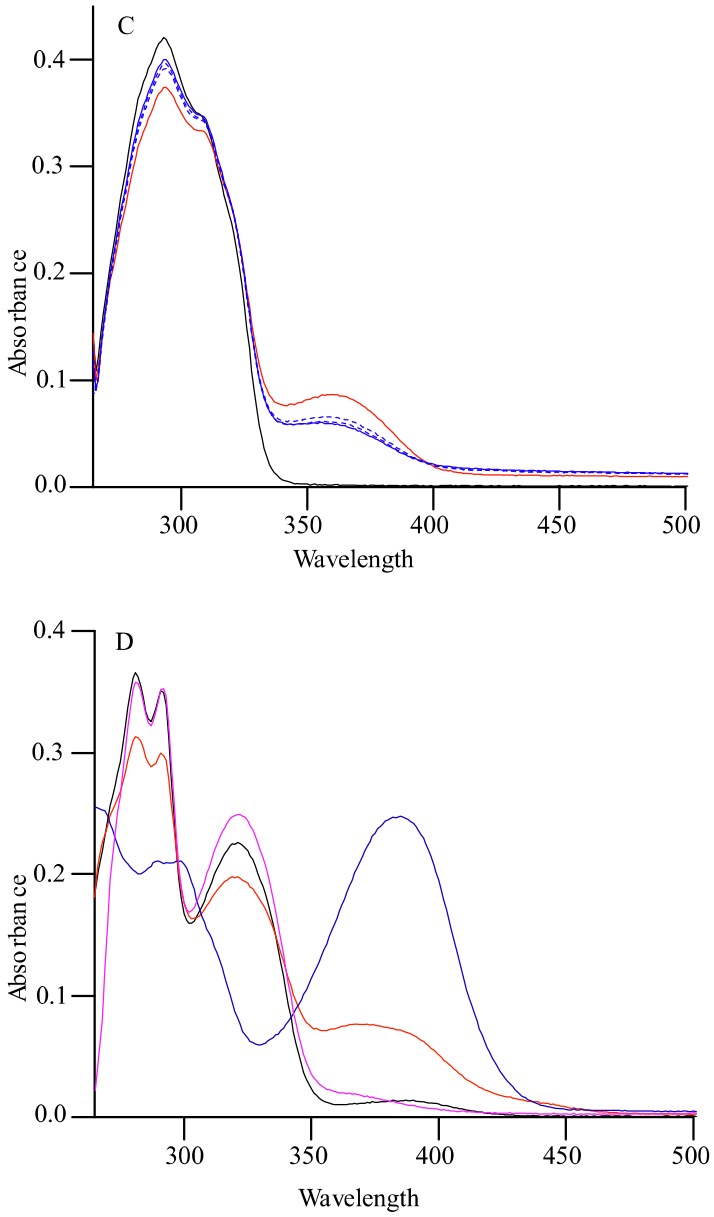

Figure 4.11 (C) Para Isomer exhibit appearance of new peak upon deprotonation while peak intensity diminishes with $Cd(OAc)_2$ addition (D) dilute acid treatment of ligand eventually blocks the binding site hence enforces to attain the ligand peak position due to protonation

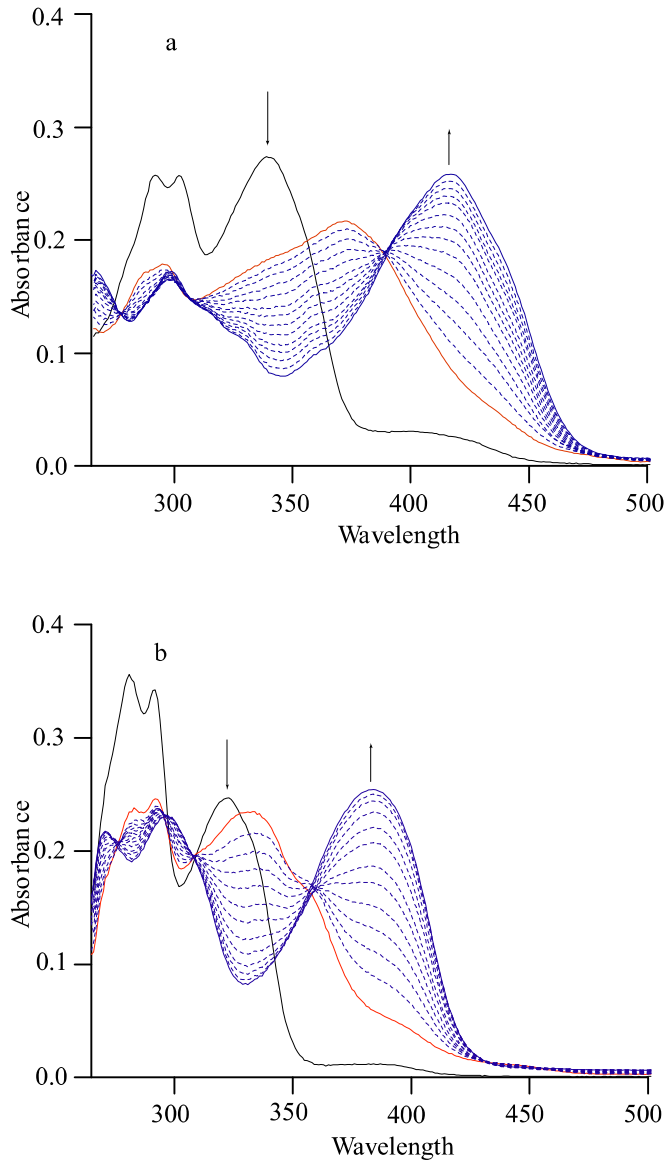

Figure 4.12 UV-vis titrations in DMF (a) ligand OL, (black line; λ_{max} 320 nm; $1x10^{-5}$ M), deprotonation with LiOH (4 equiv., red line) and upon aliquot addition of $Cd(OAc)_2$ (blue line) band corresponding to ligand diminishes ratio-metrically with appearance of new peak at 418 nm along with fine isosbestic point, similar titration experiment with (b) ligand ML

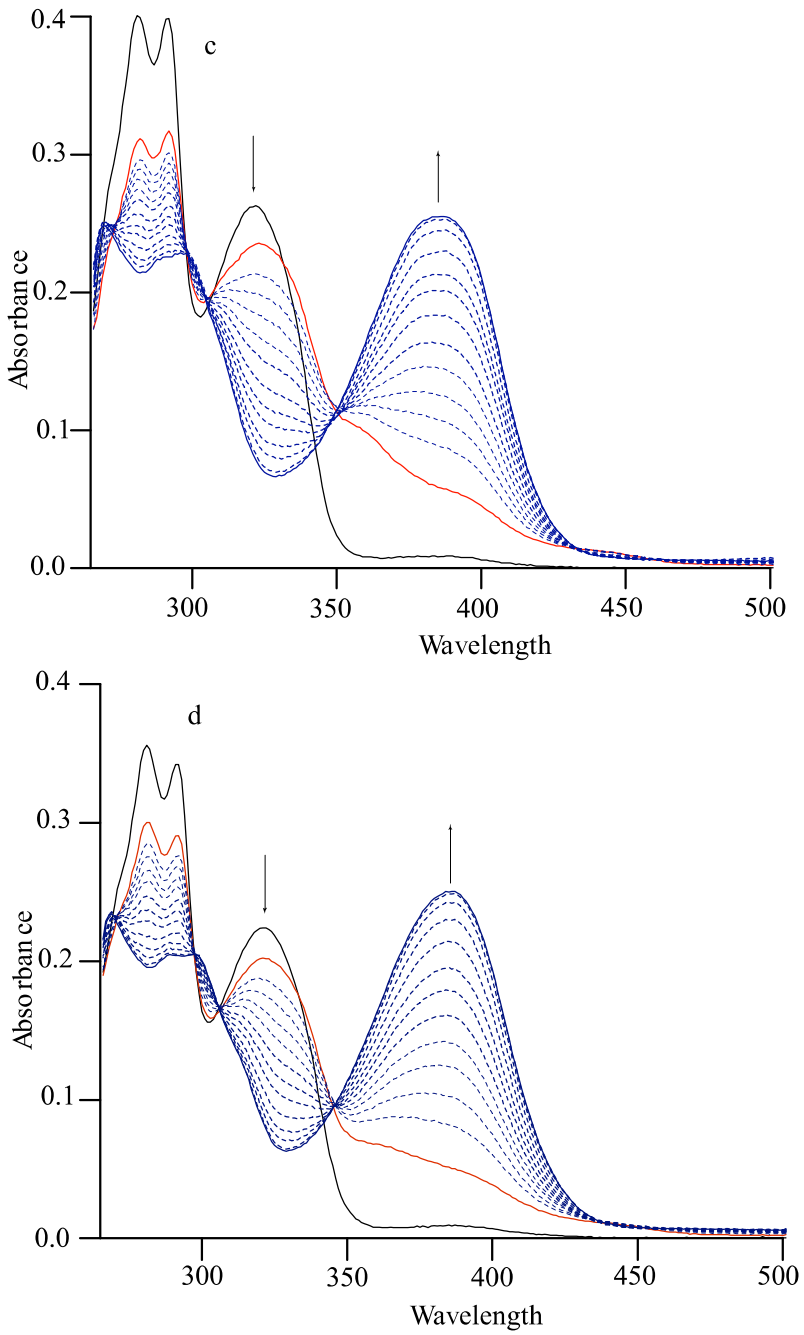

Figure 4.13 UV-vis titrations in DMF (a) ligand OL, (black line; λ_{max} 320 nm; $1x10^{-5}$ M), deprotonation with LiOH (4 equiv., red line) and upon aliquot addition of $Cd(OAc)_2$ (blue line) band (c) ligand SL, (d) ligand GL

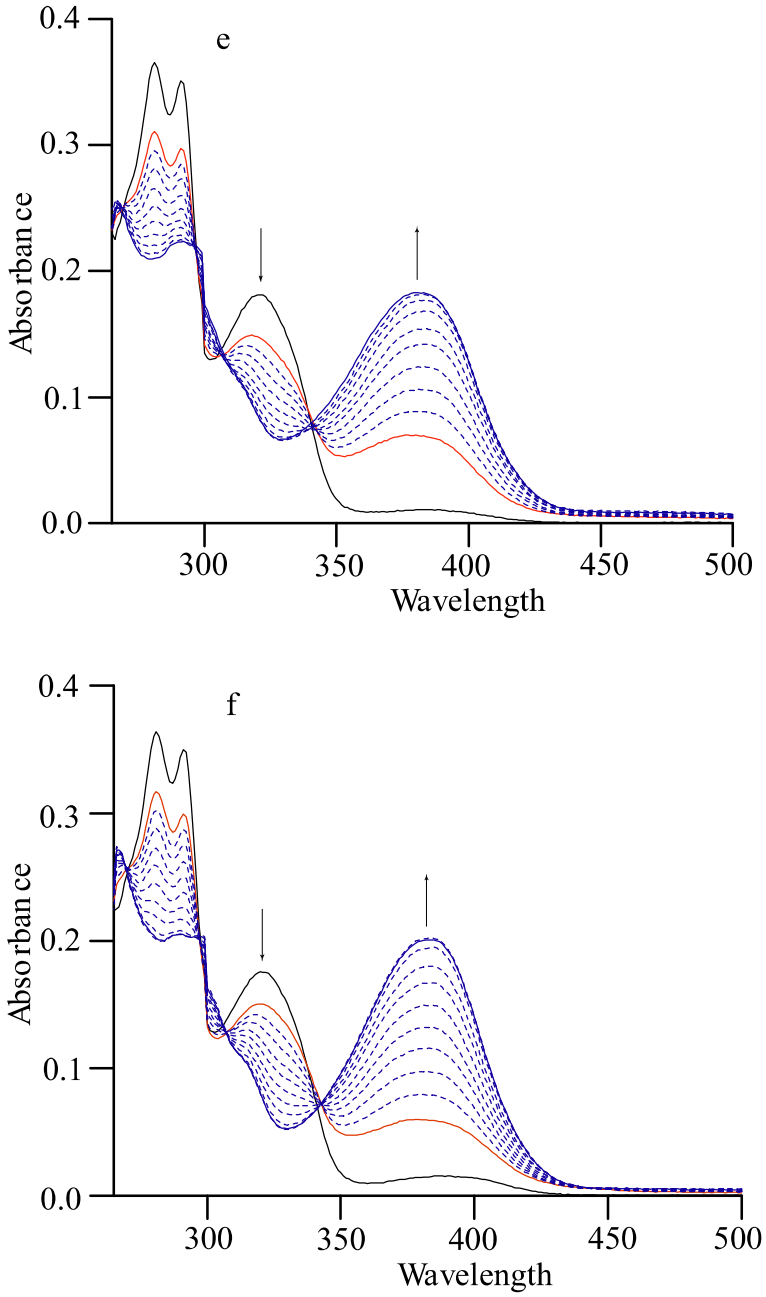

Figure 4.14 UV-vis titrations in DMF (a) ligand OL, (black line; λ_{max} 320 nm; 1x10^{-5} M), deprotonation with LiOH (4 equiv., red line) and upon aliquot addition of Cd(OAc)$_2$ (blue line) band (c) ligand PL, (d) ligand SUL

4.3.11.1 Supporting UV-vis Spectroscopy

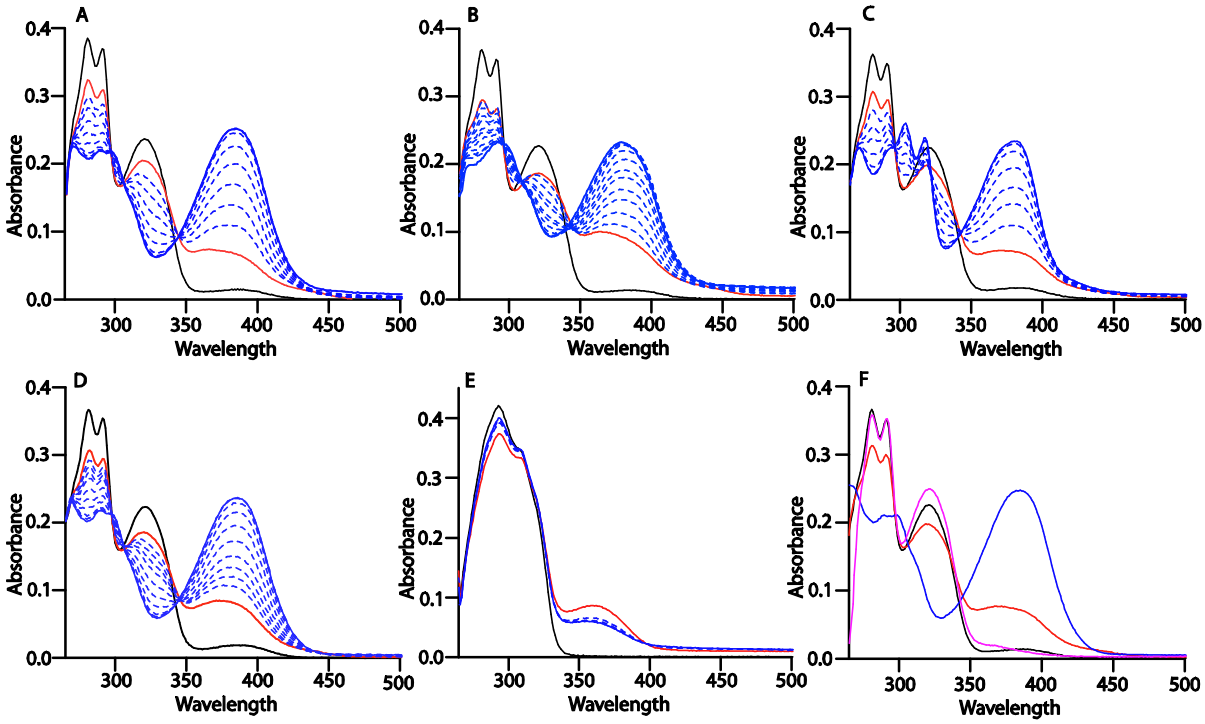

Figure 4.15 UV-vis titrations in DMF (A) ligand AL (black line; λ_{max} 322 nm; $1x10^{-5}$ M), deprotonation with LiOH (2 equiv., red line) and upon aliquot addition of $Cd(OAc)_2$ (blue line) band corresponding to ligand diminishes with appearance of new band at 378 nm, coincidently with an isosbestic point; similar titration experiments performed with (B) $Zn(OAc)_2$ and (C) $Cu(OAc)_2$ (D) $Cd(NO_3)_2$ shows nearly similar peak position, but variation in fluorescence behavior discussed later signify role of acetate ion towards aggregation and in turn gelation (E) Para Isomer exhibit appearance of new peak upon deprotonation while peak intensity diminishes with $Cd(OAc)_2$ addition (F) dilute acid treatment of ligand eventually blocks the binding site hence enforces to attain the ligand peak position due to protonation

Job's plot for all isomers

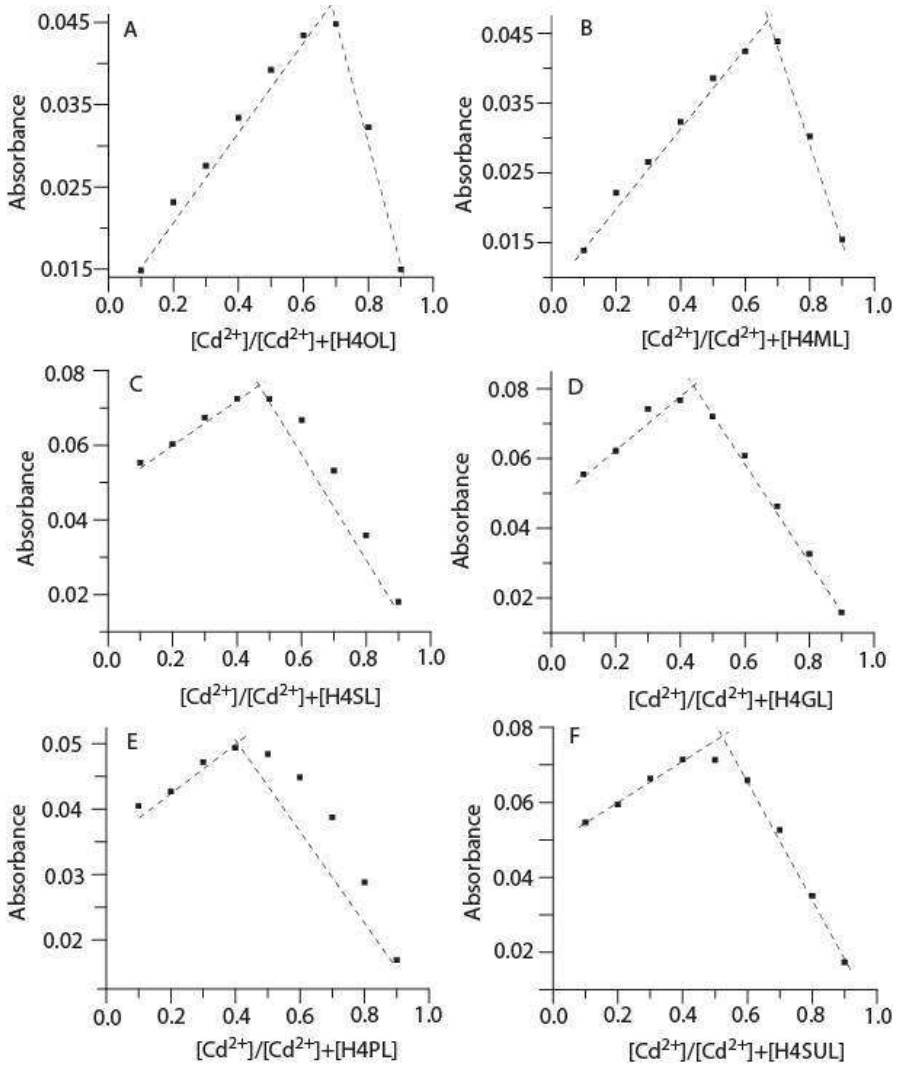

Figure 4.16 Job's plot of all homologues with Cd^{2+} in the presence of LiOH

Table 4.3 Job's Plot ratio $[Cd^{II}]/[Cd^{II}]+[Ligand]$ of various ligands under similar titration conditions to adipic

Ligand	OL(A)	ML(B)	SL(C)	GL(D)	AL(gelator)	PL(E)	SUL(F)
Job's Plot ratio	**3:2**	**3:2**	**1:1**	**1:1**	**1:1**	**2:3**	**1:1**

4.3.12 Fluorescence Study

Upon dilution of metallogel emission peak at 480 nm displayed a large blue shift of ~24 nm in two successive steps viz. photoluminescence intensity quenching (observed in the range of 10^{-2} to 10^{-3} M) and its enhancement (for 10^{-3} to 10^{-4} M dilution) which in turn indicates the presence of aggregation. In terms of fluorescence intensity quenching and its enhancement during gel dilution advocated the presence of two interesting phenomenon viz. AIE followed by ACQ in the gelation process.

Under similar conditions, the non-fluorescent behavior of Para isomer clearly indicates the role of phenolic –OH over ortho position upon emission behavior and gelating ability. As gelation was observed only in H_4SL and H_4AL (zig-zag conformation were found to be energetically more stable) where both of them shown marked decrease in emission upon Cd (II) addition, H_4SUL having a similar trend of emission behavior lack gelation ability may be due to its larger spacer size.

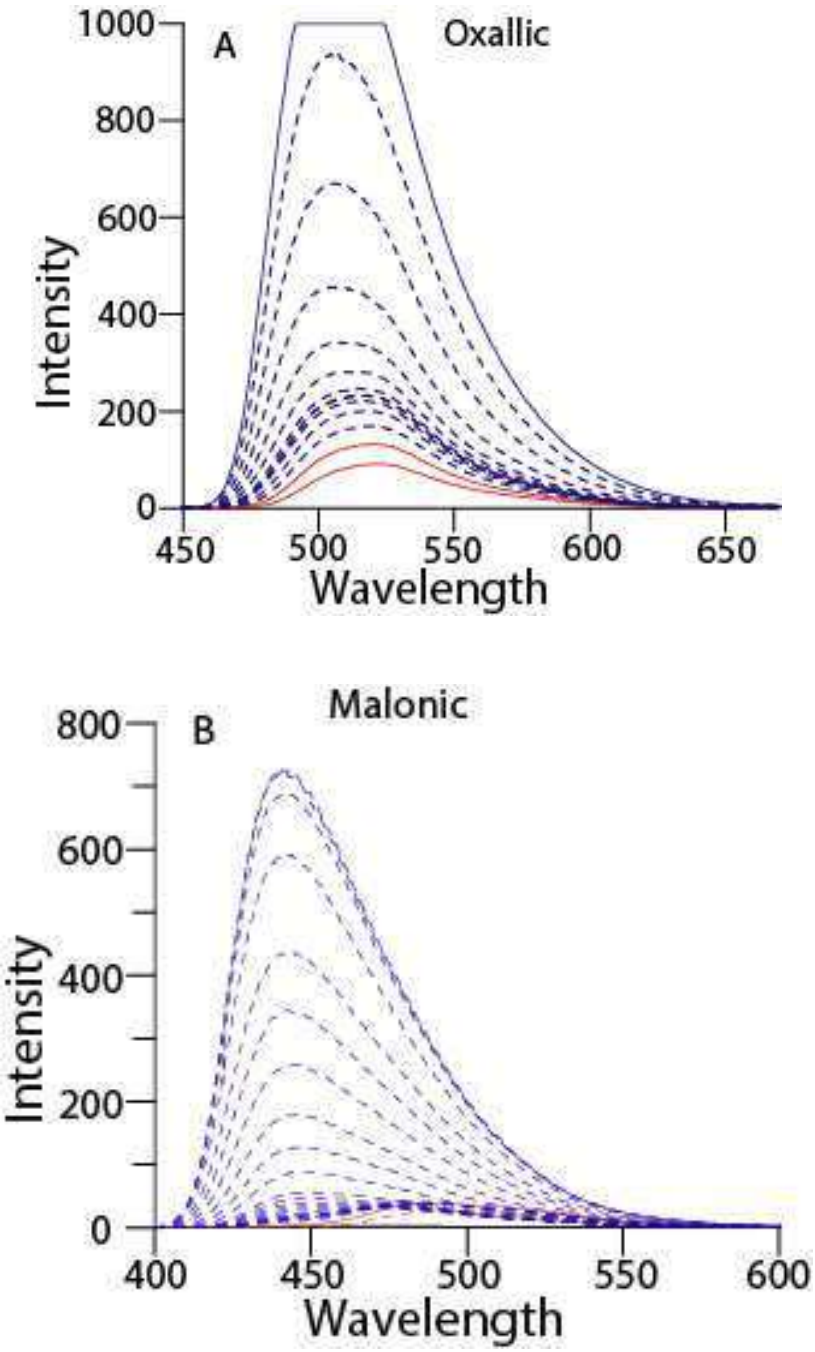

Figure 4.17 Fluorescence spectra in DMF (Red line = deprotonated ligand, Blue line = Metal addition) (A) Oxallic ligand (λ_{ex} = 339 nm), (B) Malonic ligand (λe_x = 322 nm)

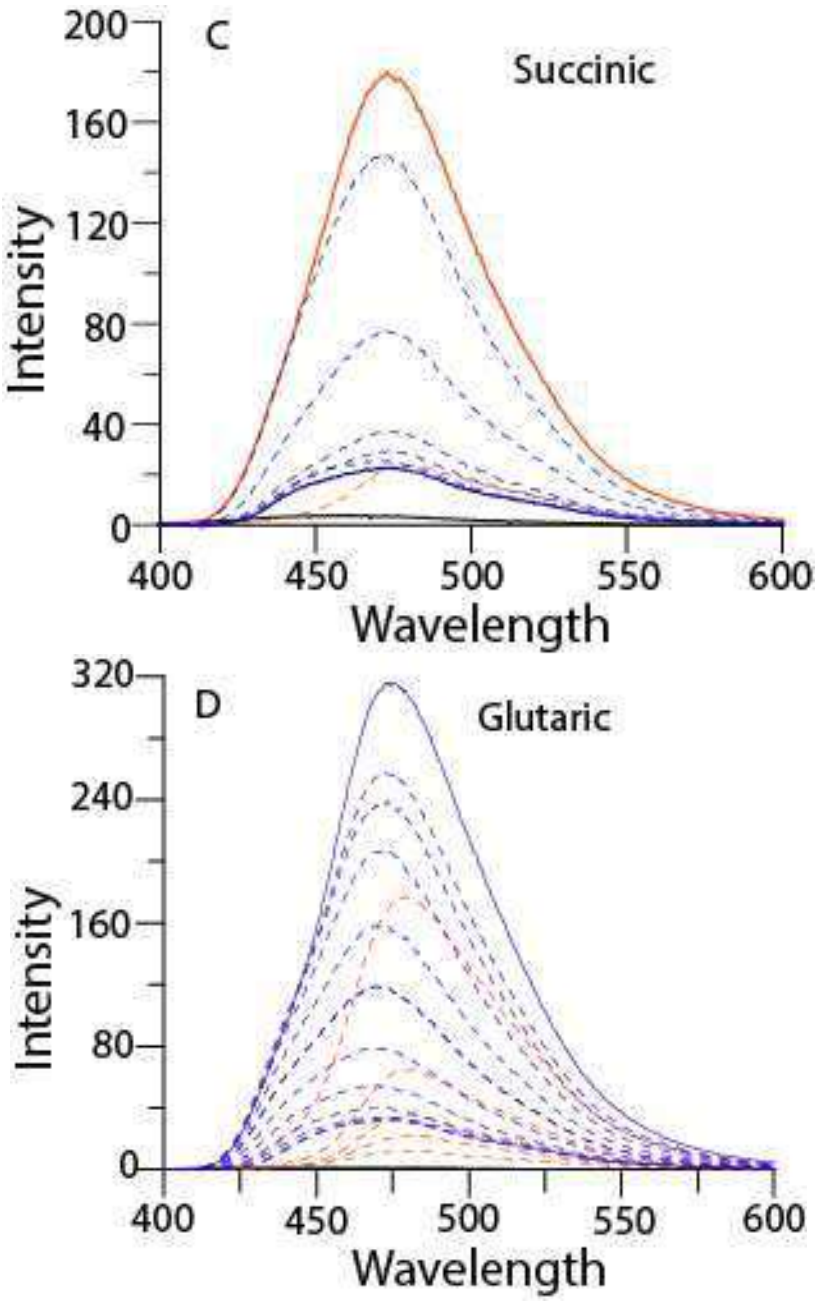

Figure 4.18 Fluorescence spectra in DMF (Red line = deprotonated ligand, Blue line = Metal addition) (C) Succinic ligand (λ_{ex} = 321 nm), (D) Glutaric Ligand (λ_{ex} = 321 nm)

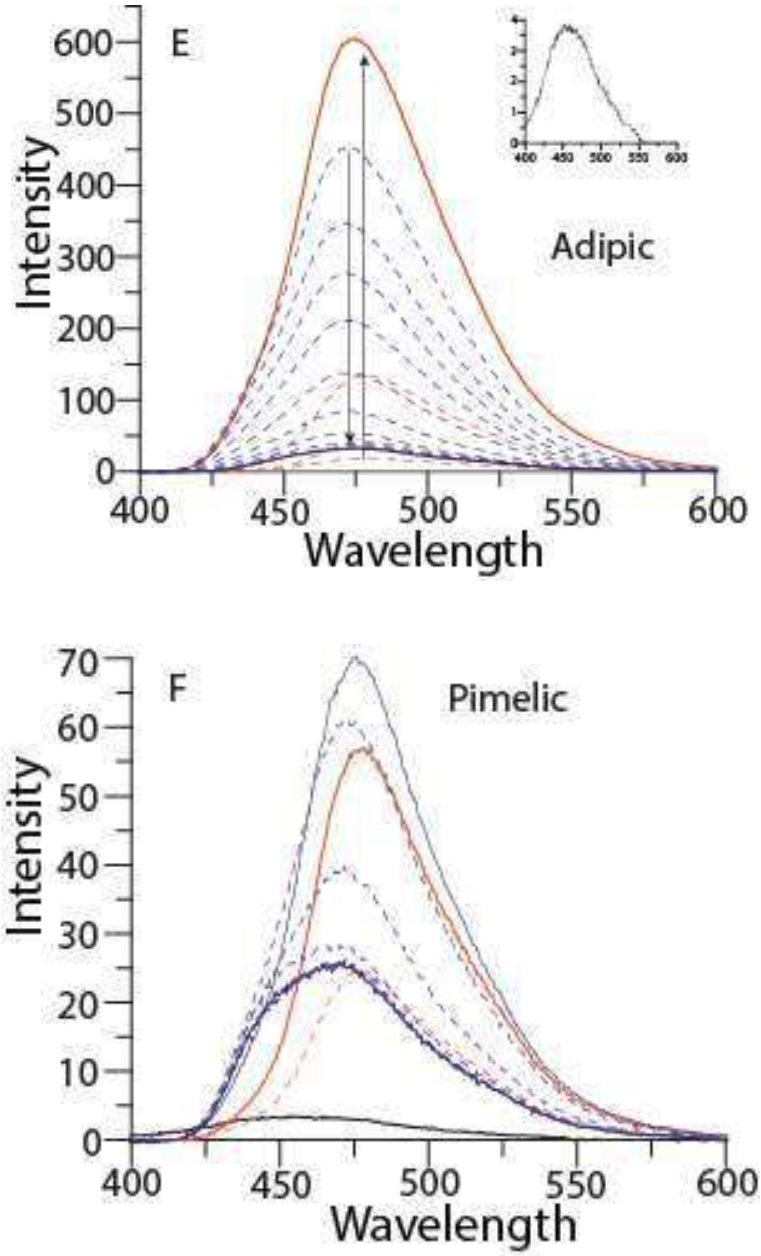

Figure 4.19 Fluorescence spectra in DMF (Red line = deprotonated ligand, Blue line = Metal addition) (E) Adipic ligand (λ_{ex} = 320 nm), (F) Pimelic ligand (λ_{ex} = 320 nm)

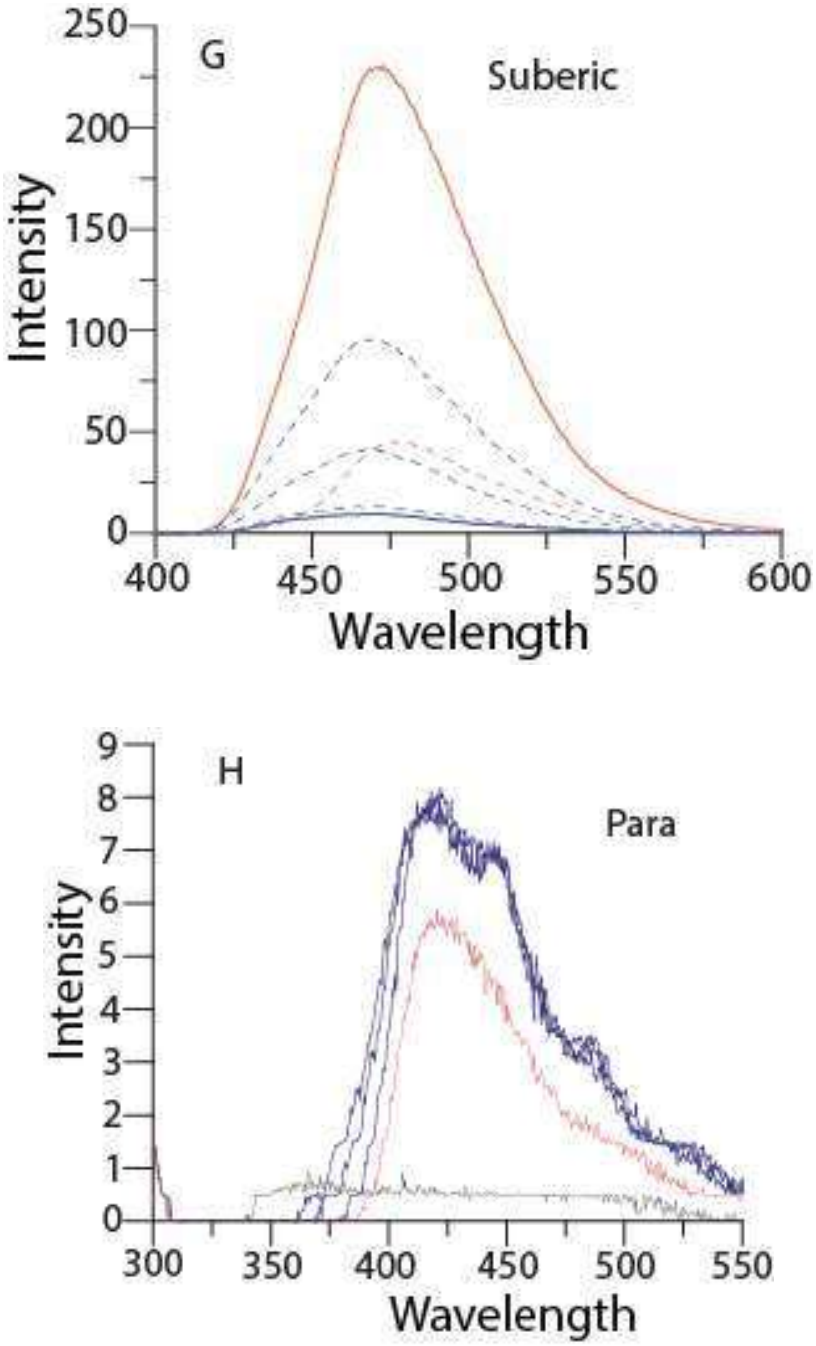

Figure 4.20 Fluorescence spectra in DMF (Red line = deprotonated ligand, Blue line = Metal addition) (G) Suberic ligand (λ_{ex} = 320 nm), (H) Para isomer (λ_{ex} = 292 nm)

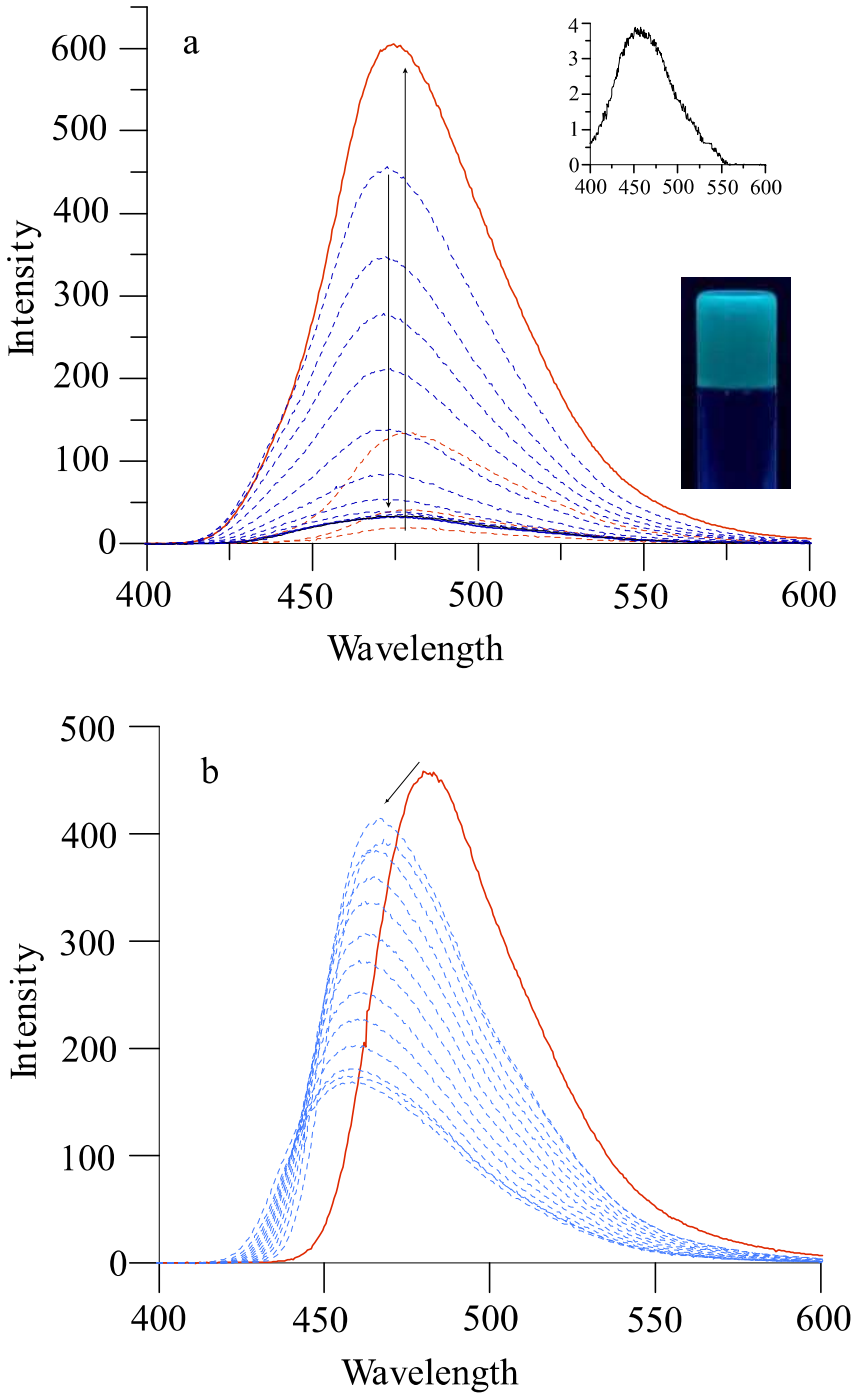

Figure 4.21 Upon dilution of gel dilution of metallogel emission peak at 480 nm displayed a large blue shift of ~24 nm (a) quenching (observed in the range of 10^{-2} to 10^{-3} M) and its enhancement (for 10^{-3} to 10^{-4} M dilution) which in turn indicates the presence of aggregation

.

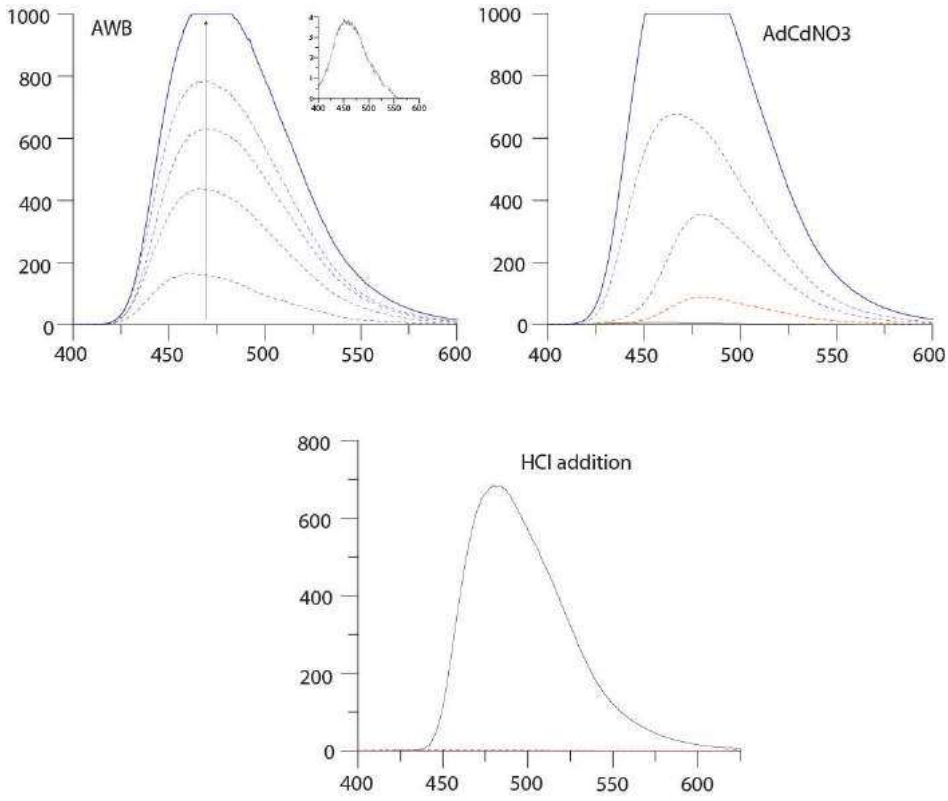

Figure 4.22 Fluorescence spectra in DMF (Red line = deprotonated ligand, Blue line = Metal addition) (A) Titration of Adipic ligand ($1x10^{-3}$ M) with $Cd(OAc)_2$ without LiOH, (B) deprotonated ligand with $Cd(NO_3)_2$, (C) Upon HCl addition to metallogel emission intensity diminishes

4.3.13 IR spectrum of H_4AL and Metallogel

FTIR spectral analysis of gelator (H_4AL) shows characteristic bands of υ(–OH), υ(–NH) at 3404 cm^{-1} and 3202 cm^{-1}, respectively, while the strong band at 1667 cm^{-1} was corroborated to υ(-C=O) group. In addition to the aforementioned peaks, υ(-C=N) is observed at 1558 cm^{-1} which suggests the enolic form of ligand. A comparative study of FT-IR spectra of gelator (H_4AL) and its xerogel suggests the disappearance of –OH band, broadening of aforementioned 'N-H' band and shifting of υ(- C=O) from 1667 to 1609 cm^{-1} ($\Delta\upsilon$ = 58 cm^{-1}) which may be attributed to coordination of Cd^{2+} through O,N,O binding core.10,11 Alkali base (4 equiv.) was required for deprotonation signifies the tetrabasic hexadentate nature of ligand as it is a necessary condition for coordination of a metal ion through deprotonation of both phenolic and -NH labile protons adjacent to azo-methine group.

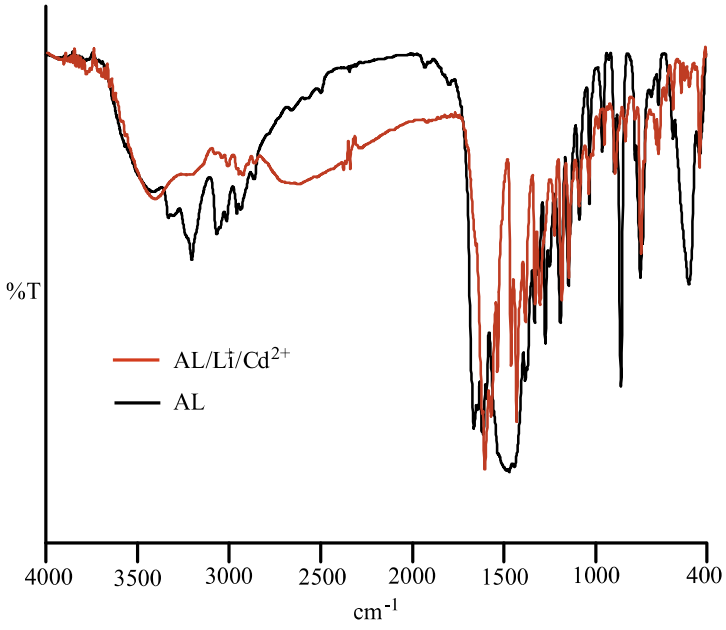

Figure 4.23 Comparative IR spectra of Gelator with Xerogel

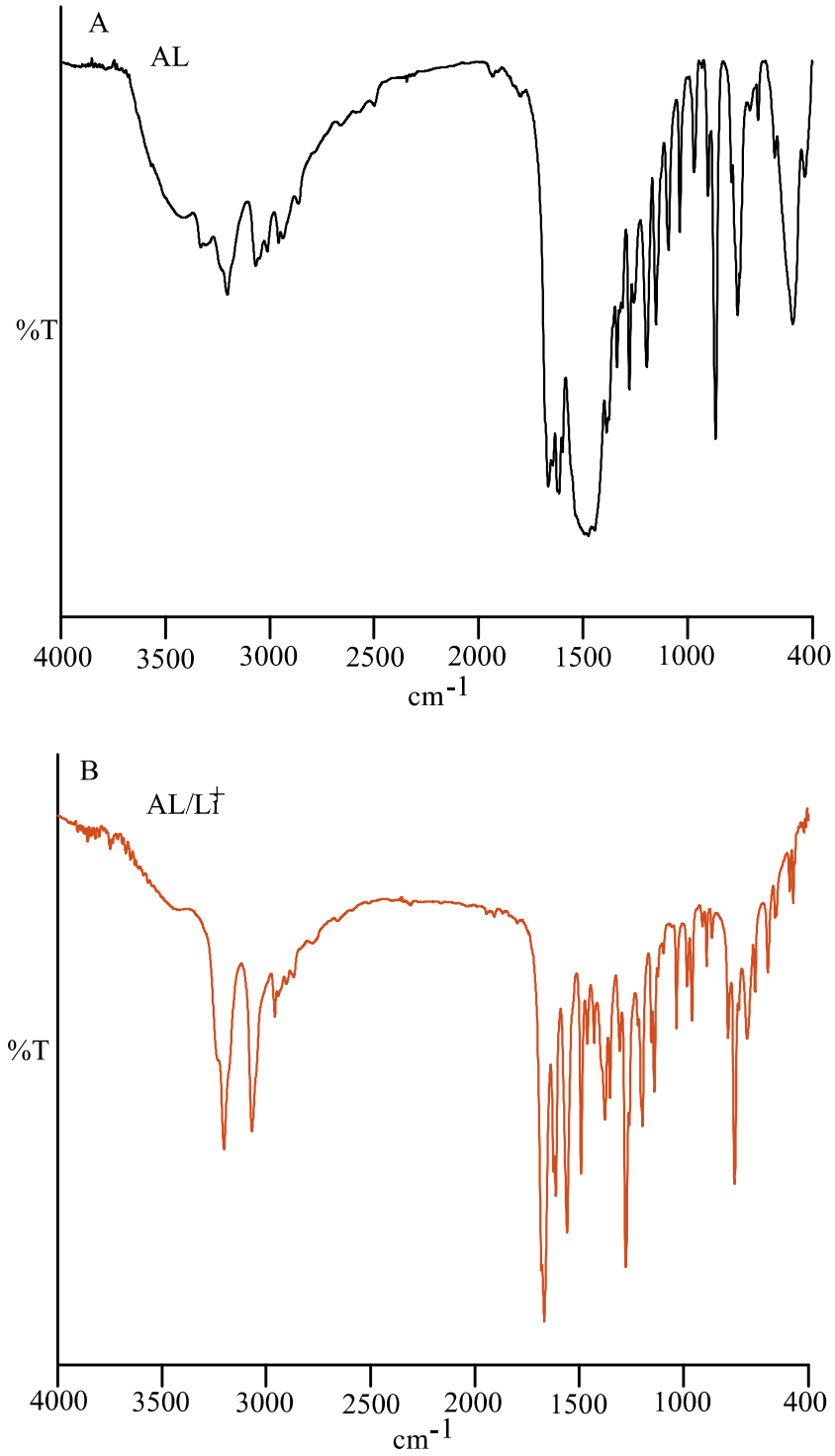

Figure 4.24 FTIR spectra for (A) Isomer AL illustrate νC=O at 1666 cm^{-1} and νC=N at 1558 cm^{-1}, (B) AL deprotonated with LiOH

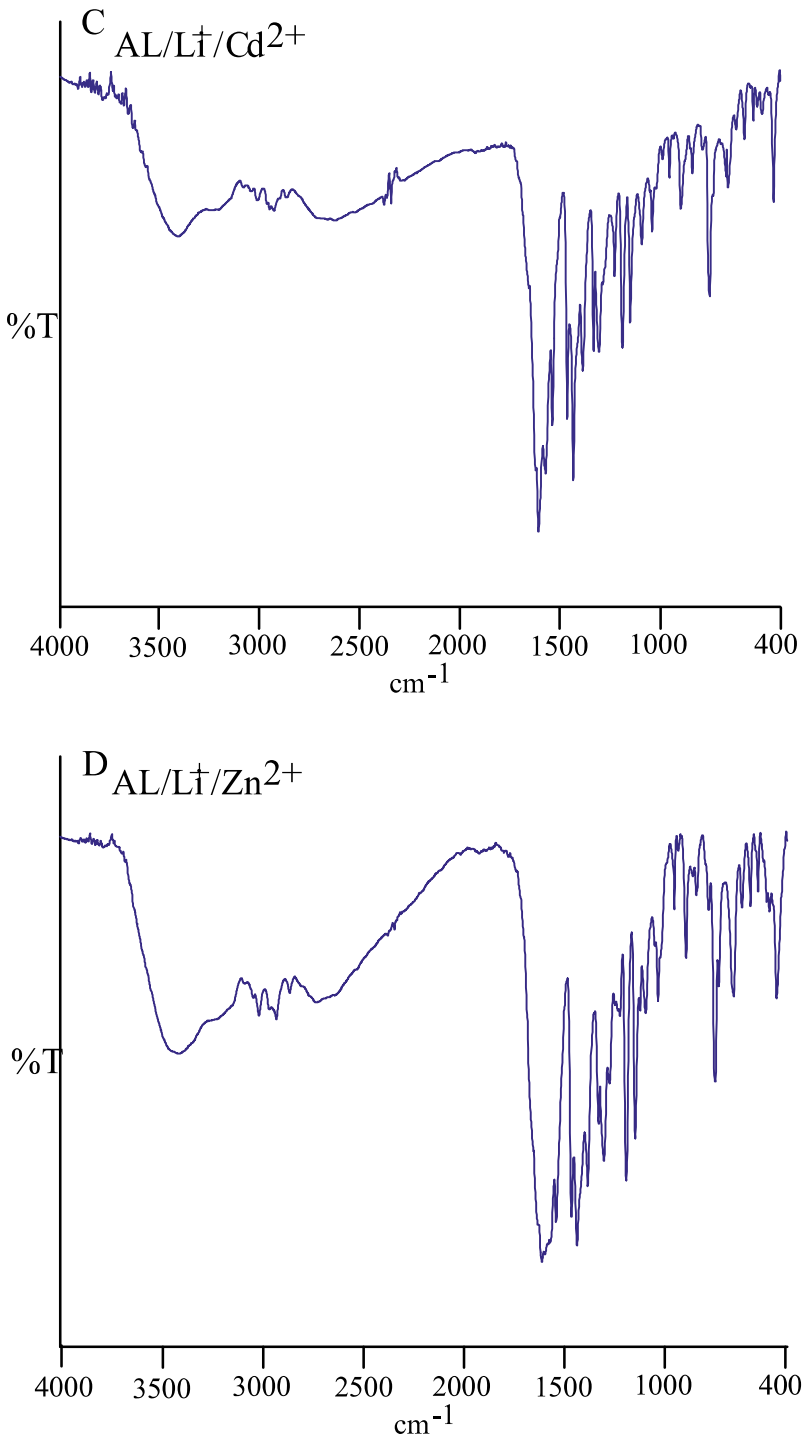

Figure 4.25 FTIR spectra for (C) xerogel indicating the down shift of ν C=O at 1609 and 1540 cm^{-1} and ν C=N at 1465 cm^{-1} and 1435 cm^{-1} which supports the binding mode of ligand with Cd^{2+} and Li^{+}, (D) AL/Li^{+}/Zn^{2+}

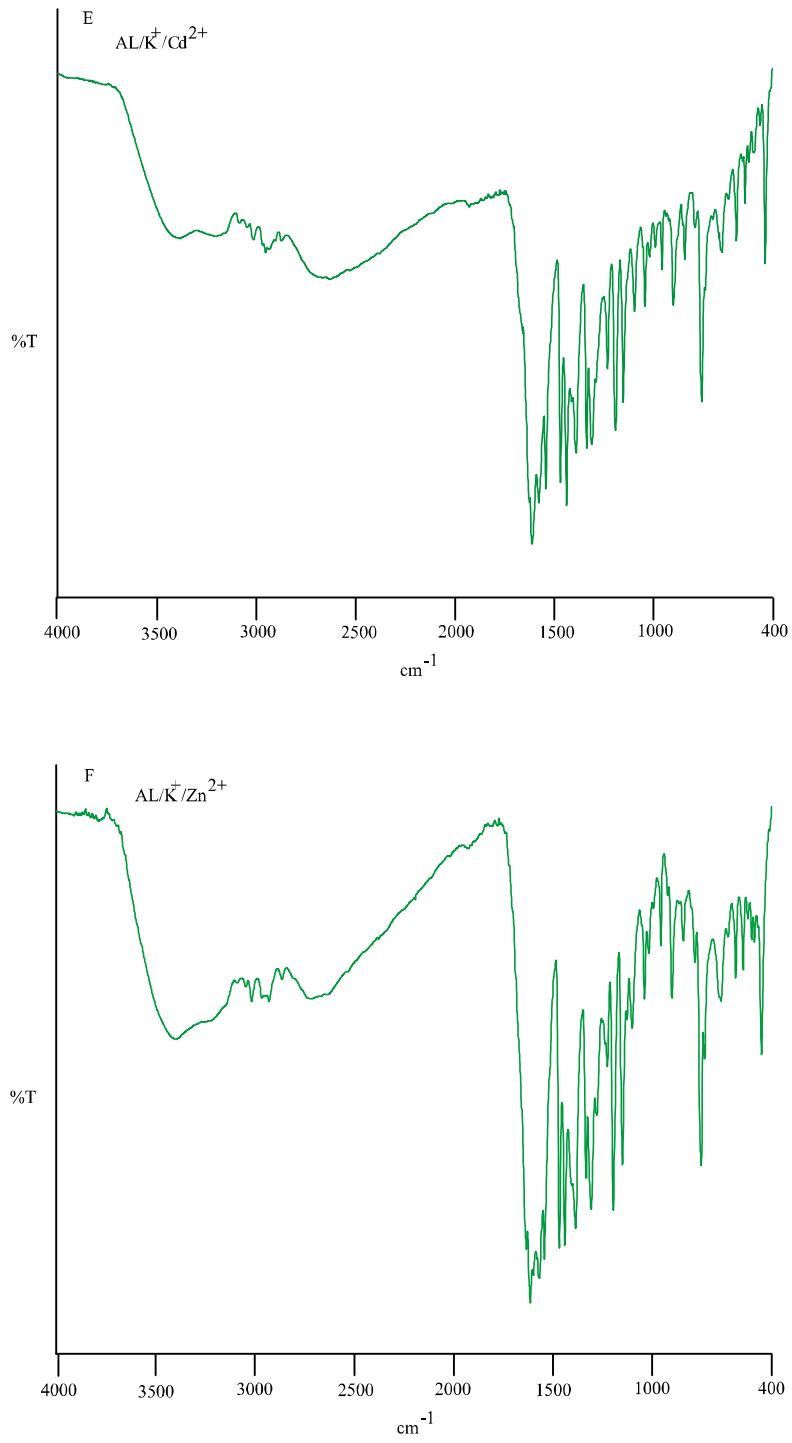

Figure 4.26 FTIR spectra for (E) AL/K^+/Cd^{2+}, (F) AL/K^+/Zn^{2+} illustrate similar binding pattern

4.3.14 comparative ESI mass spectrum of gelator and metallogel

In order to prove the coordination polymeric nature indicated by Job's plot, we have performed detailed ESI-MS spectral analysis of diluted metallogel. In ESI-MS spectra, the base peak was observed for gelator $[C_{20}H_{22}N_4O_4\text{-}H]^-$ at m/z= 381.15 (calcd. 381.15). Another significant peak was observed in diluted metallogel for $[C_{20}H_{20}N_4O_4Cd\text{-}H]^-$ at m/z= 493.04 (calcd. 493.04). ESI-MS spectrum for $[C_{20}H_{20}N_4O_4Cd\text{-}H]^-$ matches nicely with simulated isotopic abundance pattern. Thus, we have found a noticeable intense peak for 1:1::H_2AL: Cd in the mass spectrum which inevitably suggested the coordination polymeric nature of metallogel. (Figure 4.27). Other gelling and non-gelling combinations also produced a similar peak for 1:1 at their respective m/z values (Figure 4.28 & 4.29) [Luisi *et al.* (2007)].

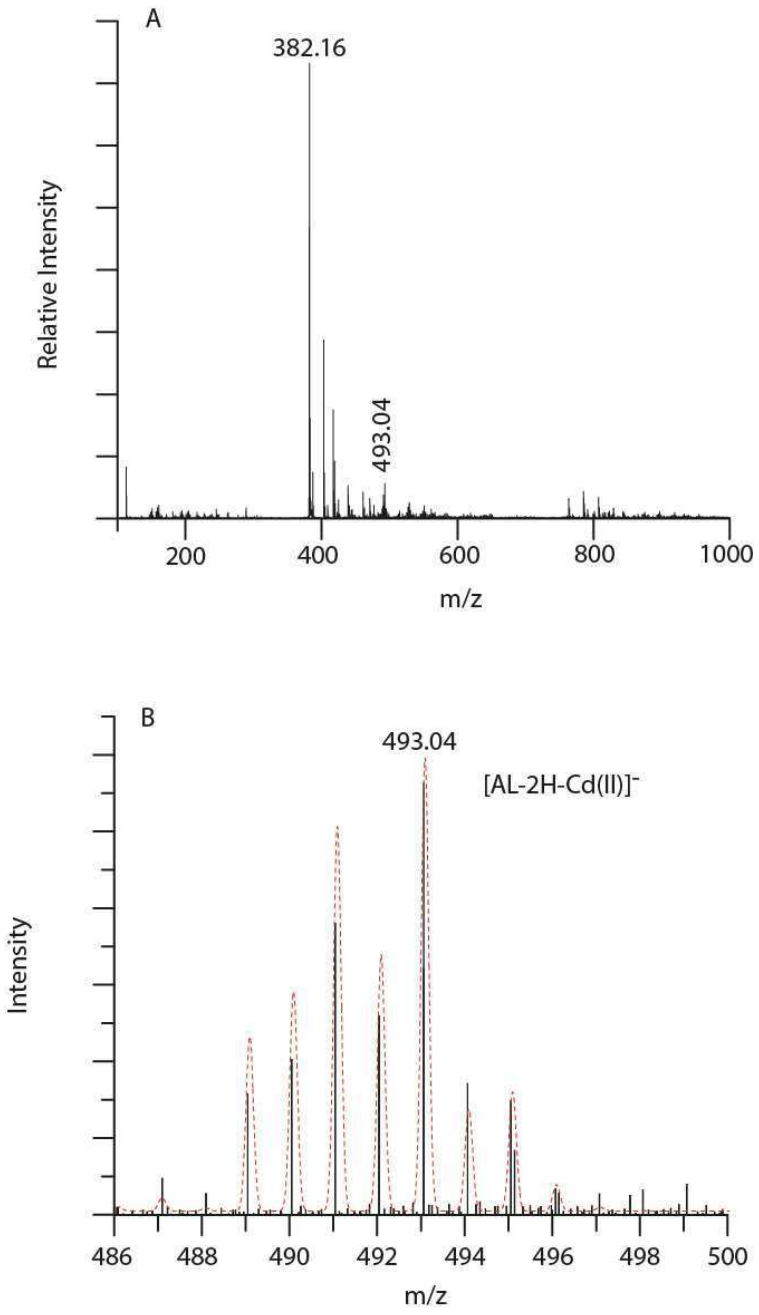

Figure 4.27 ESI-MS (DMF) spectra of (A) diluted metallogel shows the molecular ion peak of AL m/z, $[1+H]^+$, 382.16 (calcd. 382.19) and metallogel molecular ion peak m/z, [AL-2H-Cd(II)-, 493.06 (calcd. 493.04) supporting the complex formation is at 1:1 ratio, (B) The experimental isotopic abundance pattern of molecular ion peak of $[AL\text{-}2H\text{-}Cd(II)]^-$ matches nicely with simulated pattern which is in accordance with Job's plot, $[1]/[Cd^{2+}] = 1:1$

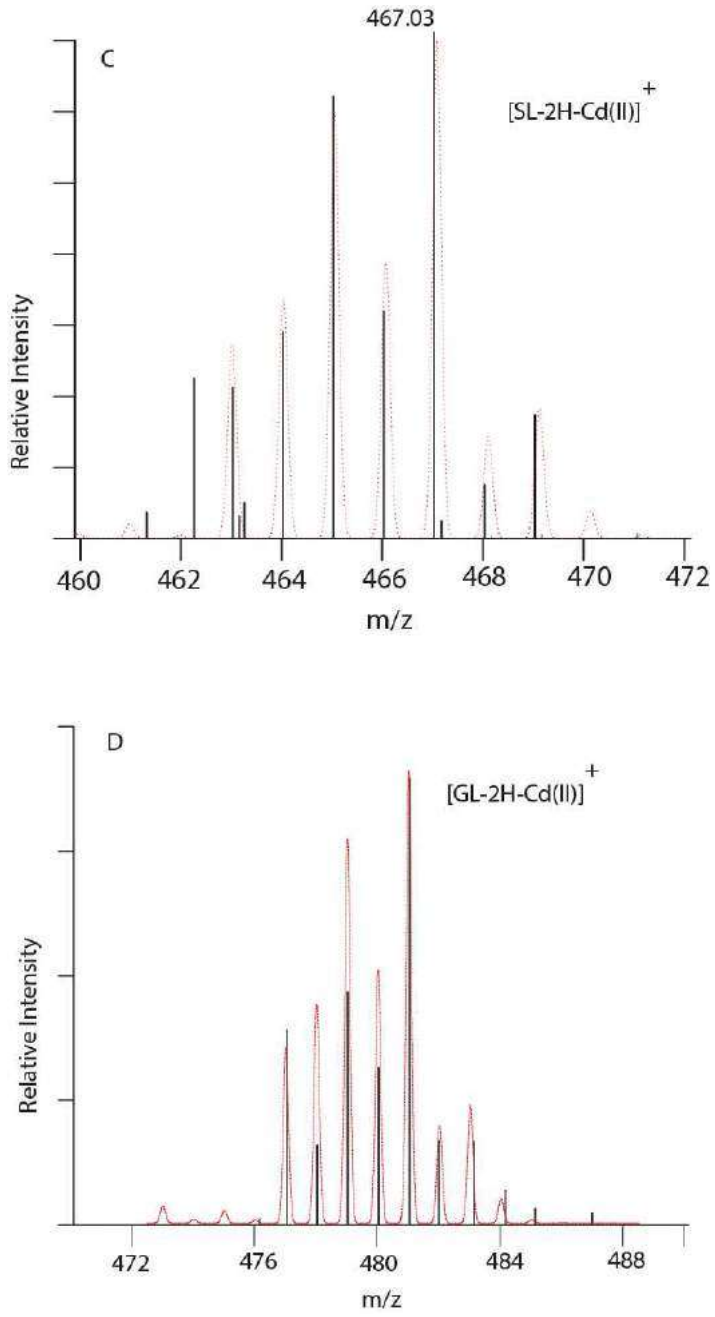

Figure 4.28 ESI-MS (DMF) spectra of (A) diluted succinic metallogel shows the molecular ion peak of m/z, [SL-2H-Cd(II)]$^+$, 467.03 (calcd. 467.04) supporting the complex formation is at 1:1 ratio, (B) diluted glutaric complex shows the molecular ion peak of m/z, [GL-2H-Cd(II)]$^+$, 467.03 (calcd. 467.04)

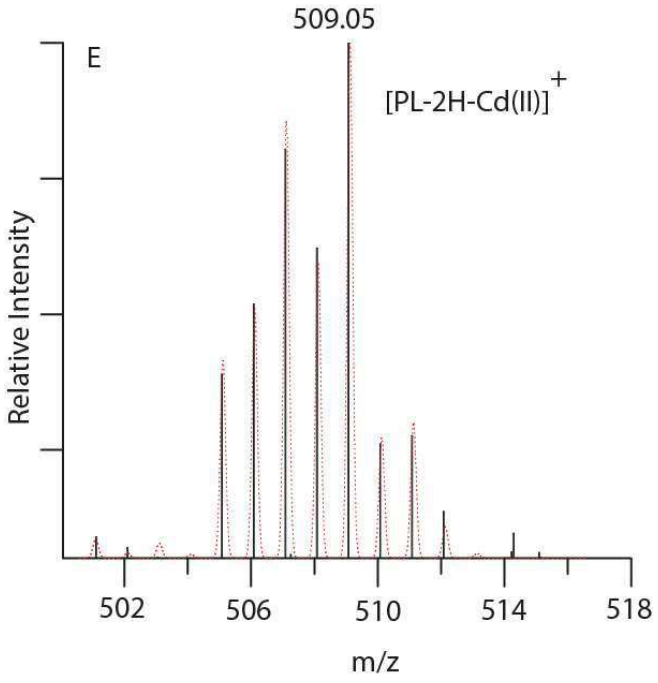

Figure 4.29 ESI-MS (DMF) spectra of diluted pimelic complex shows the molecular ion peak of m/z, $[PL\text{-}2H\text{-}Cd(II)]^+$, 509.05 (calcd. 509.05) supporting the complex formation is at 1:1 ratio, supporting the complex formation is at 1:1 ratio, matches nicely with simulated pattern which is in accordance with Job's plot

4.3.15 Lifetime study of various gelator and non-gelling combination

Average Lifetime values determined for gelling combinations along with non-gelling combinations pointed out the effect of the spacer on emission as well as gelation behaviour. The fluorescence decay value of metallogel yields value of 1.423 ns while that observed for deprotonated ligand was 3.143 ns suggesting strong non-radiative interaction of excited states of the deprotonated system. On the other hand, non-gelling combinations like H_4GL and H_4PL under similar conditions displayed lifetime values of 1.88 ns and 2.27 ns, respectively upon metal addition where no large decrease in lifetime value is observed with respect to deprotonated ligand (Figure 4.30 & 4.31). This observation may signify the relation between the AIE effect and fluorescence lifetime values with the length of spacer [Xue *et al.* (2016)].

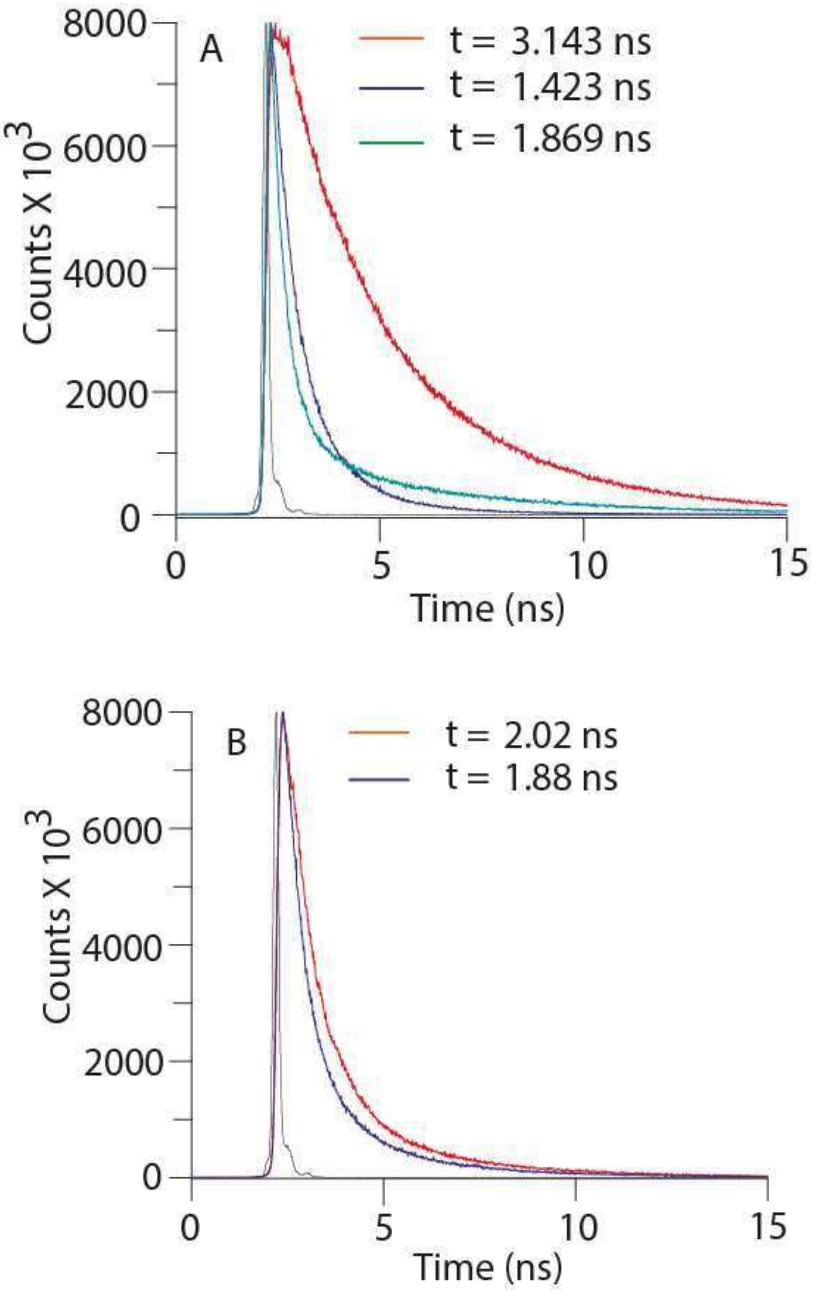

Figure 4.30 Lifetime measurements of deprotonated homologues (A) adipic ligand, (B) glutaric ligand (red line = deprotonated ligand; blue line = $Cd(OAc)_2$; green line = $Zn(OAc)_2$

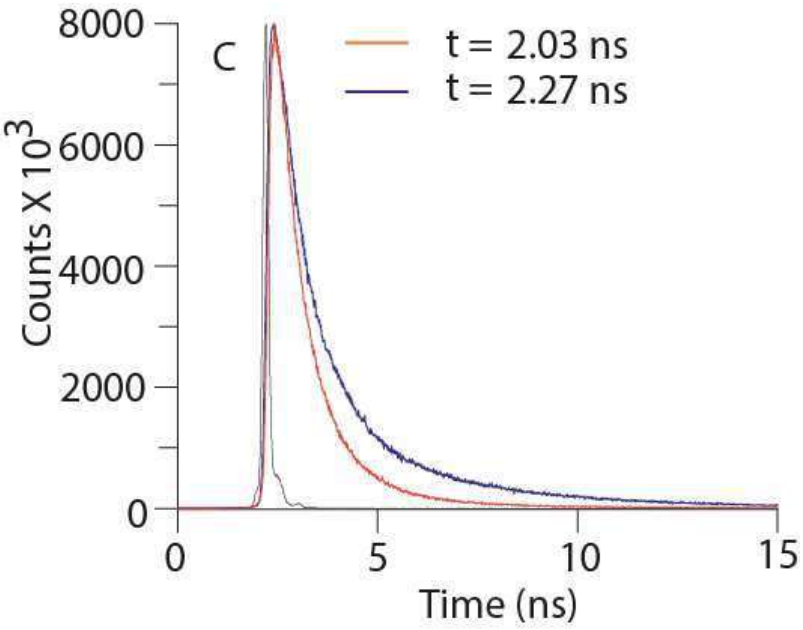

Figure 4.31 Lifetime measurements of deprotonated homologues (C) pimelic ligand (red line = deprotonated ligand; blue line = $Cd(OAc)_2$; green line = $Zn(OAc)_2$

4.3.16 Binding mode obtained from Job's plot and ESI mass spectra

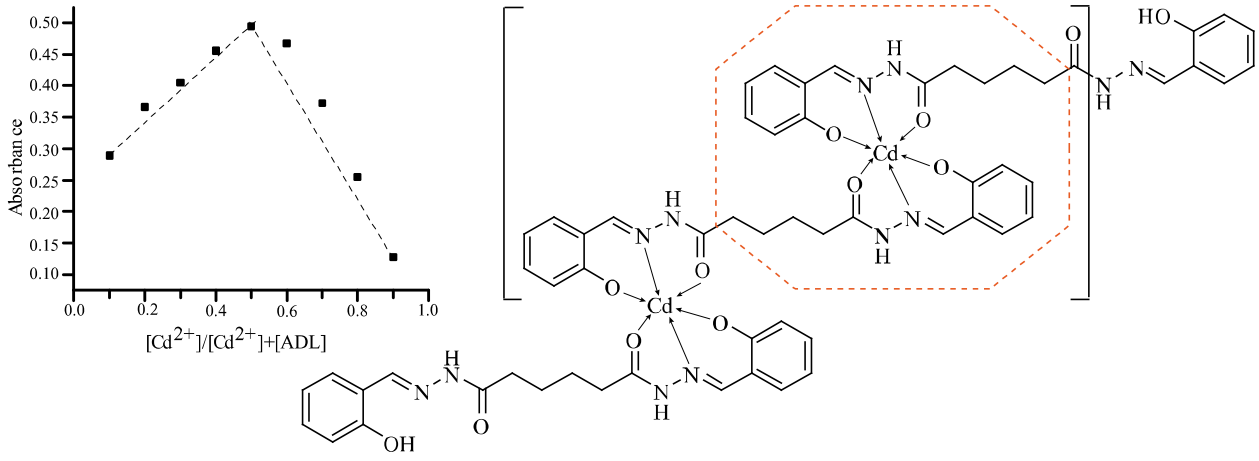

Figure 4.32 Job's plot for LiOH deprotonated AL vs. $Cd(OAc)_2$ showing 1:1 stoichiometry performed in DMF, [Cd(II)]/[Cd(II)]+[AL] vs. absorbance monitored at 378 nm. (B) The 1:1 stoichiometry suggests that the possible complex may be coordination polymer as demonstrated through sketch diagram along with asymmetric unit highlighted through Dotted (red) circle

4.3.17 TGA analysis

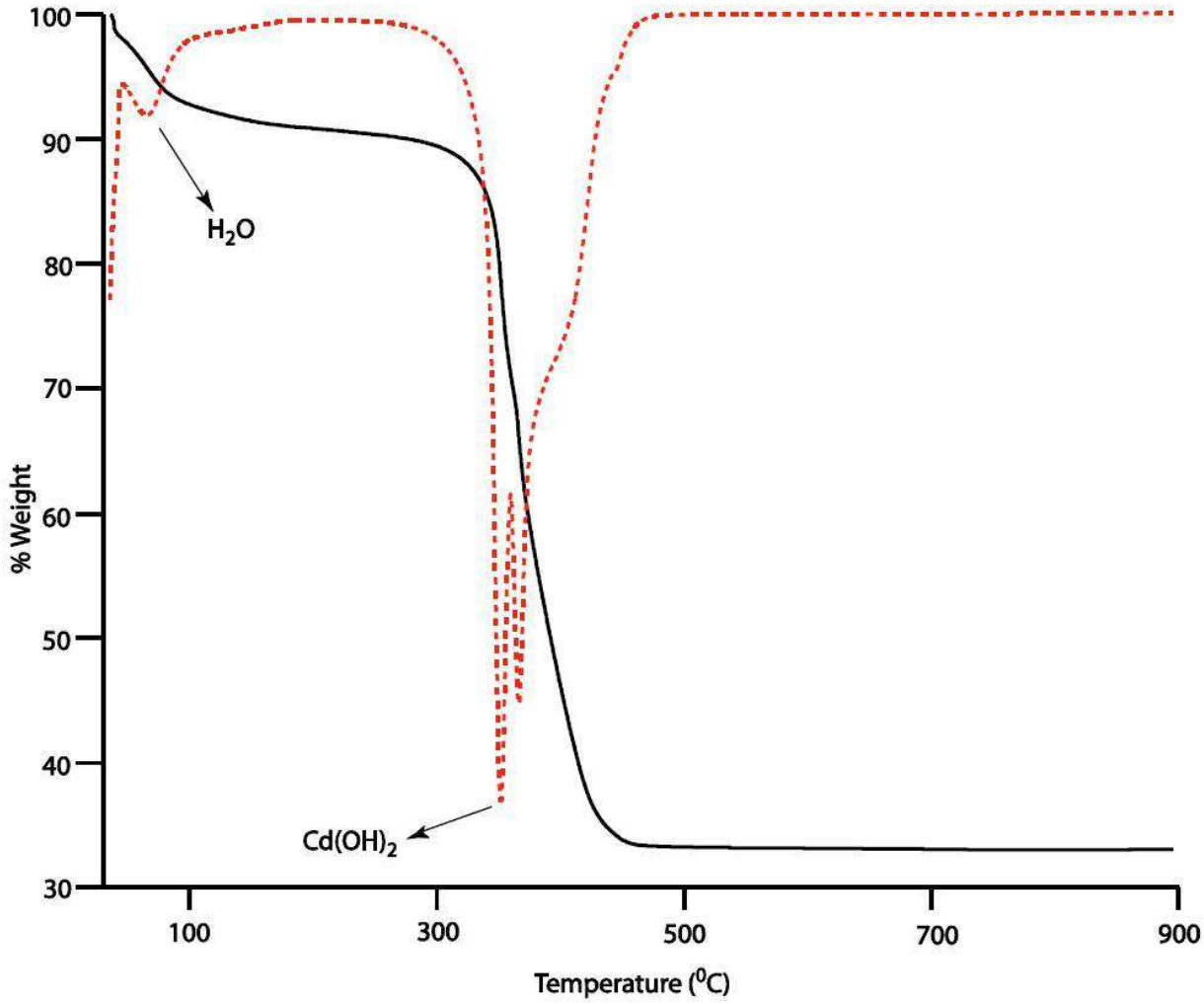

Figure 4.33 The Thermo Gravimetric Analysis (TGA) of isolated compound from xerogel (washed with H_2O to remove any extra salt and vacuum dried) along with derivative plot shows 4.35% and 32.9% weight loss within the temperature range 40−320° C, which suggests loss of one lattice water and one $Cd(OH)_2$ molecules, respectively (weight loss as per TGA: 4.35 % (calcd. for H_2O 3.66 %); 32.9 % (calcd.for $Cd(OH)_2$ 29.89 %) and 34.32 % are corresponding to various kind of degradation of complex)

4.3.18 Rheology

In order to acquire mechanical properties of metallogel various rheological studies were performed. Rheological experiments were conducted over freshly prepared (1.0% w/v) fixed concentration metallogel. Implementation of frequency sweep measurements between 0.1 and 100 rad s^{-1} at 25°C within the linear viscoelastic region indicated that G' and G'' values were linear and increase slightly within the applied frequency (f) range (-1.0-2.0 rad s^{-1}) principally supporting its elastic nature. Furthermore, G' is dominating G'' and they do not cross each other, suggesting no phase separation or transition which is anticipated for a stable and rigid gel phase material. Further evidence of elasticity was visualized by the fact that G' and G'' are very less sensitive to angular frequency (ω). At secondary axis, double logarithmic plot of η* (dynamic viscosity) with ω shows a gradient close to -1, indicating constant viscosity declination (Figure 4.34). Variation tendency of both storage modulus (G') and loss modulus (G'') with increasing temperature were recorded from temperature range 25-160°C. As shown in (Figure 4.35 b), both values remain unaffected up to 100° C and above which both G' and G'' decreases with inclination in temperature, indicating liquefaction. Storage Modulus (G') and loss modulus (G") are obtained at 25°C and 1 rad s^{-1} as a function of shear stress and strain (Figure 4.35 a). Metallogels when subjected to oscillatory shear, value of G' was found be higher than G'' by order of ~1 magnitude of shear stress. This is in accordance to the true gel phase where no variation among G' and G'' was observed with appreciable long range of increasing applied stress. At a yield stress of ~1.6 Pa G' and G'' intersect each other establishing a mechanical breakup of gel beyond which the deviation from linearity results in gel-sol phase transition. On the other hand both in-phase storage modulus (G') and out-of-phase loss modulus (G'') remain constant up to

1.1% (G'>G''), beyond which deformation of network occurred. Temperature responsiveness and thermal stability of metallogel was observed by plot between loss tangent (δ=G''/G') *vs.* temperature where a considerable change at 100°C indicate phase transition temperature "T_{gel}" (Critical temperature) (Figure 4.36 c). The dynamic temperature ramp result concludes that phase transition occurs through the gel-solid, at nearly 100°C which is expected for the gel formed in DMF (Figure 4.36 d).

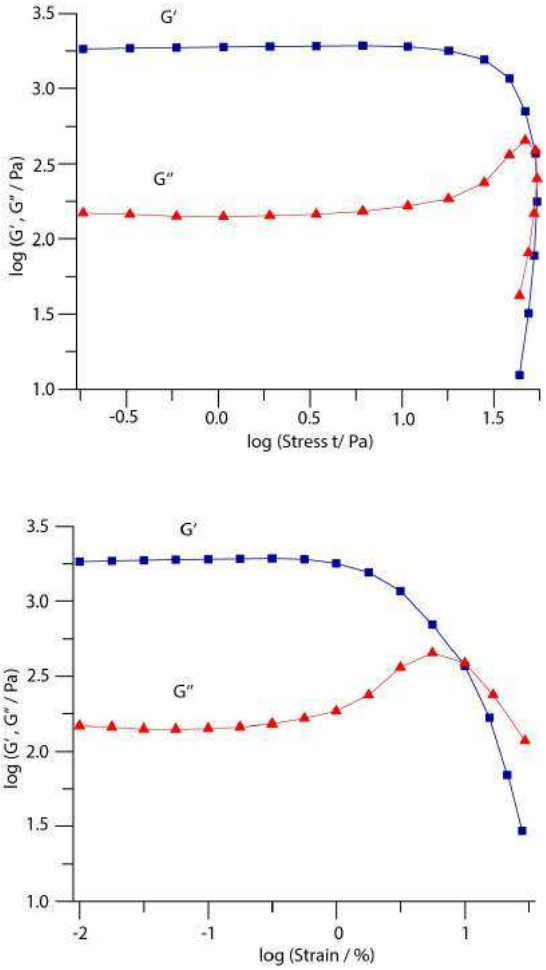

Figure 4.34 (upper) dynamic shear stress of G' and G'' for gel and (lower) Dynamic oscillation strain sweep of G' and G'' for gel at a frequency of 1 rad s^{-1} and 25° C

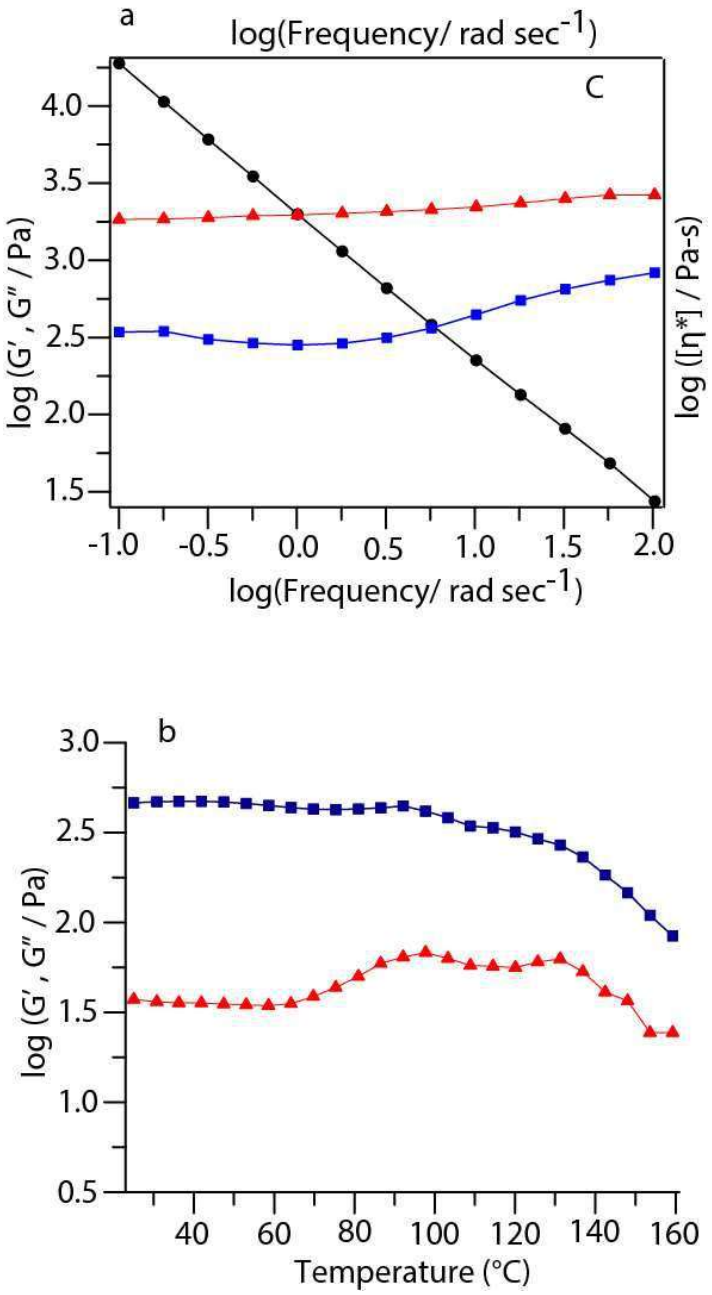

Figure 4.35 (a) Dynamic frequency sweep measurement of G' and G'' for Cd gel at strain of 0.5%. Secondary axis: complex viscosity measurements and (b) Dynamic temperature ramp G' and G'' for Cd gel at heating rate of 1°C min^{-1}, strain of 0.5% and frequency of 1 rad s^{-1}

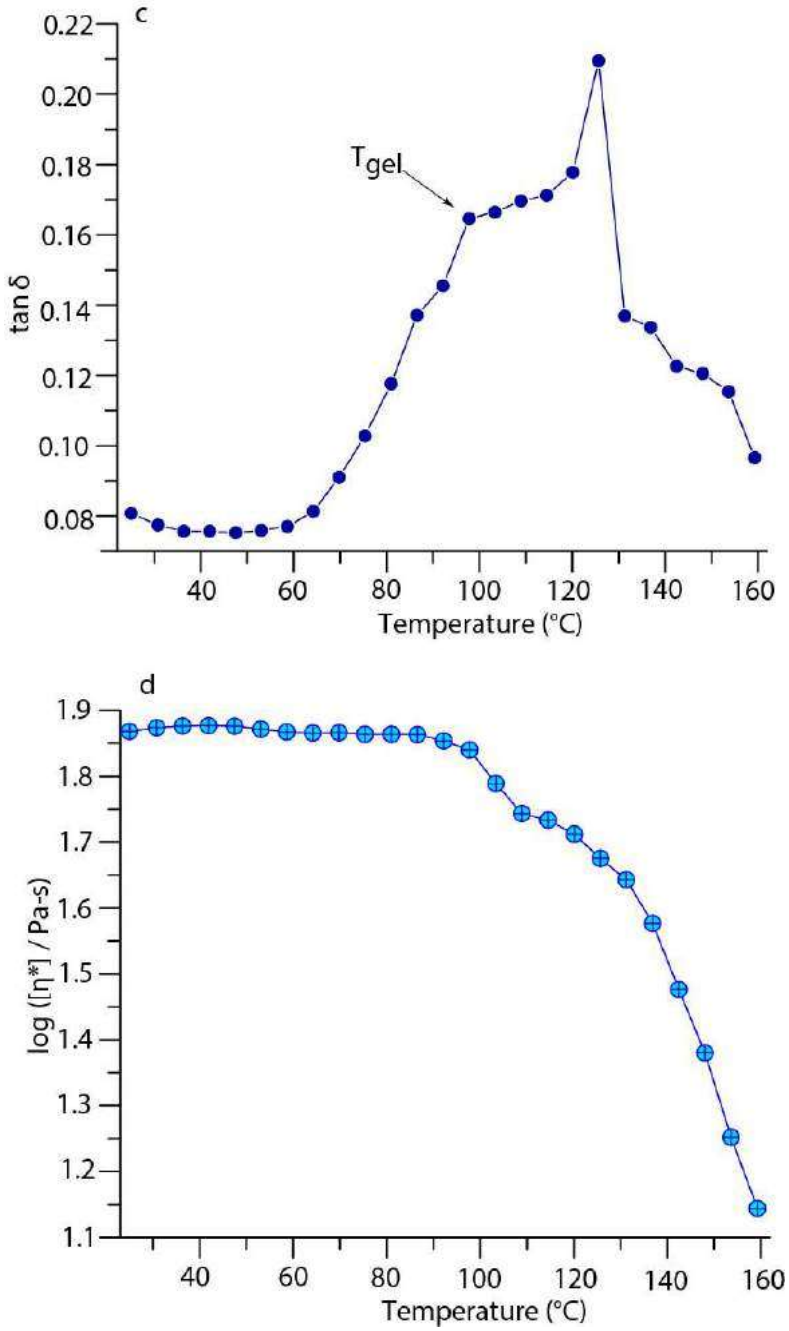

Figure 4.36 (c) Dynamic temperature ramp of loss tangent (tanδ =G"/G') plot at 5°C min^{-1}, which indicates the critical temperature (T_{gel}) 100 °C for metallogel and (d) Dynamic temperature ramp of complex viscosity measurement at 5 °C min^{-1}

4.3.19 plausible mechanism

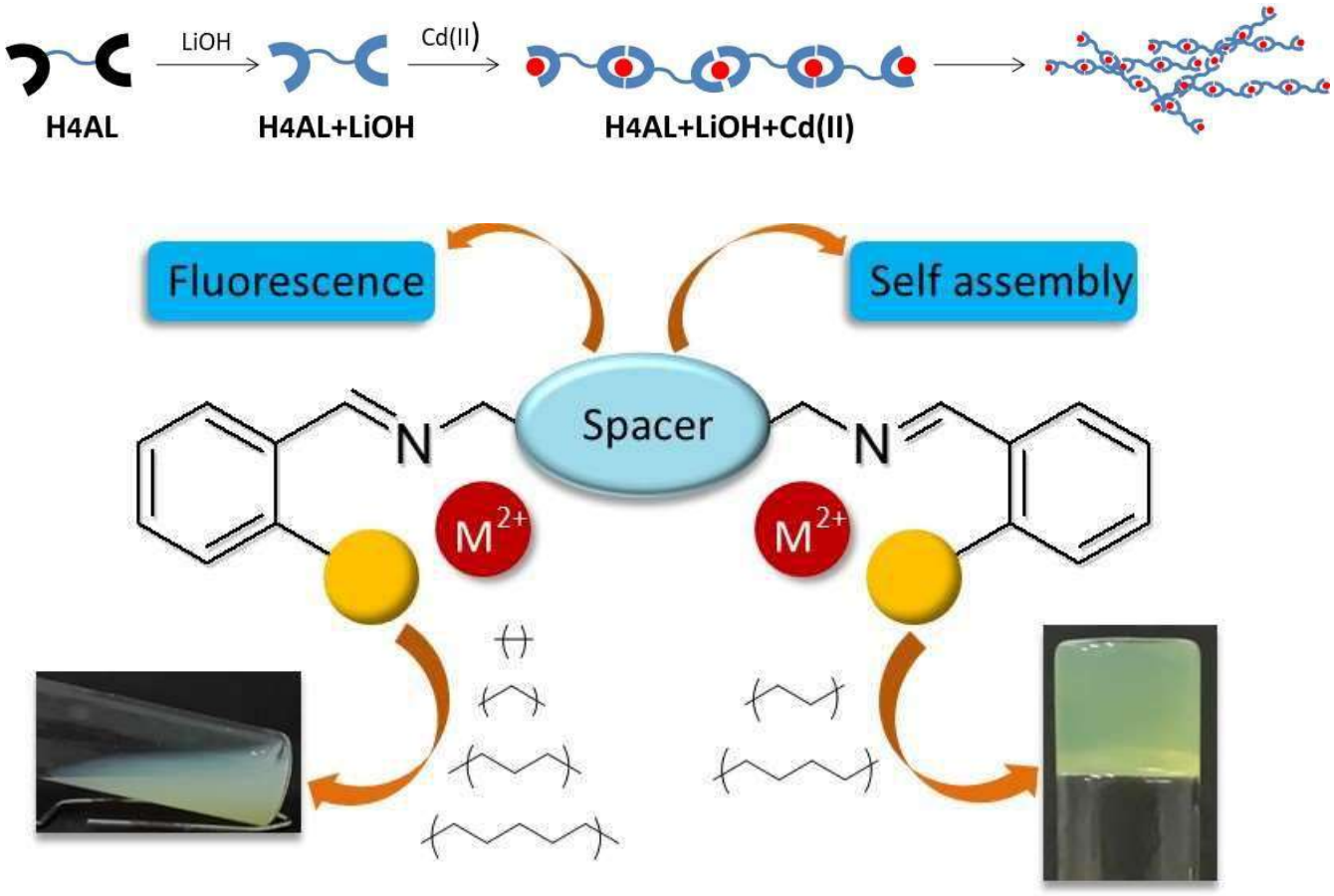

Figure 4.37 plausible mechanism and summary of gelation clearly indicating the role of alkyl chain length in gelation behavior and formation of Coordination polymer in metallogel

4.4 Conclusion

In conclusion (Figure 4.37), this article has taken account of a series of homologous bipodal derivatives, where gelation behavior and photophysical properties were explored in correlation to spacer length. The non-emissive solution of the gelator became emissive upon deprotonation followed by metal addition due to CHEF along with the AIE-ACQ effect. Obtained results emphasize that the legitimacy of spacer length along with cation and anion

play an important role in realizing systems towards gelation ability. The gelation mechanism is well established by UV-vis, FT-IR, Job's plot, PXRD, fluorescence, lifetime measurements and TEM experiments. Rheological experiments accomplished over metallogel and verified to be true gel phase material. The current itinerary of the synthesis of metallogel might be expedient in the exploration of new fluorescent metallogel materials in the upcoming time.